Isogeometric Model Reconstruction of Open Shells Via Ricci Flow and Quadrilateral Layout-Inducing Energies

Kendrick M. Shepherd[a,*], Xianfeng David Gu[b], Thomas J. R. Hughes[c]

[a]*Department of Civil and Environmental Engineering, Brigham Young University, Engineering Building 430, Provo, UT, 84602-4081, U.S.A*
[b]*Department of Computer Science, Stony Brook University, New Computer Science Building, Stony Brook, NY, 11794-2424, U.S.A*
[c]*Oden Institute for Computational Engineering and Sciences, The University of Texas at Austin, 201 East 24th Street, C0200, Austin, TX, 78712-1229, U.S.A.*

This paper is dedicated to Professor Herbert Mang in honor of his numerous scientific contributions, his long and dedicated service to the international engineering community, and in celebration of his 80^{th} birthday in January 2022.

Abstract

Isogeometric analysis has received extensive attention in the last decade, but despite its merits, many isogeometric models are still produced manually or semi-manually. In this work, we introduce a new technique using Ricci flow and a carefully constrained minimization to convert trimmed and faceted open geometries into watertight spline models free of trim and suitable for isogeometric analysis with potential for automation. This technique is used to rebuild parts of the US Army's DEVCOM Generic Hull vehicle and portions of a 1996 Dodge Neon finite element model into trim-free spline models. Isogeometric modal analysis is performed on each to show the viability of this reconstruction framework in generating IGA-suitable splines for shell analysis.

Keywords:
Quadrilateral layout, global parameterization, spline reconstruction, trim, shell analysis, isogeometric analysis, computer-aided design

1. Introduction

Engineering shell structural analysis requires an integrated design-through-analysis framework. Under the current paradigm, a designer creates computer-aided design (CAD) geometry to define the intended shape by combining a set of smooth B-spline or NURBS patches into a so-called "boundary representation" or "B-Rep" (which may simply be a midsurface, or "open" B-Rep); an analyst then replaces it with a finite element mesh that only approximates the original CAD geometry. Not only is the precise geometry of the model lost in this procedure (which alone may have significant implications [53]), but underlying physics of the analysis may also be lost. Additionally,

*Corresponding author
Email addresses: kendrick.m.shepherd@byu.edu (Kendrick M. Shepherd), gu@cs.stonybrook.edu (Xianfeng David Gu), hughes@oden.utexas.edu (Thomas J. R. Hughes)

this process takes a significant amount of time (over 70% of the design-through-analysis process) [6, 27] and money [11]. Regarding the analysis of these faceted meshes, traditional finite element techniques for shells struggle with locking (which is alleviated by increasing polynomial degree [2]) and numerically-induced large spurious eigenvalues (which increase with increased polynomial degree [40]). For operations such as explicit dynamics, where the maximal time step is inversely proportional to the square root of the maximum eigenvalue [4, p. 335], increasing polynomial degree leads to a reduction of time step size and a concomitant increase in computational effort.

Isogeometric analysis (IGA), proposed in [39], aims to address these issues by using the same smooth basis functions employed in CAD for engineering analysis. Isogeometric techniques can be used to directly solve (without resorting to mixed methods) high order PDEs like the Kirchhoff-Love shell formulation [45, 61] and to represent physics using smooth spline functions [39, 40]. Isogeometric methods are more accurate per degree of freedom than traditional finite element methods [25, 73, 74] and can operate directly on the B-spline and NURBS geometries created in CAD without the need for an auxiliary faceted mesh [36, 39]. Furthermore, the smoothness of isogeometric basis functions alleviate modal "outliers" introduced with traditional finite element techniques [41, 64, 73], and increasing basis function smoothness and polynomial degree accordingly reduces locking [3, 62, 92, 93]. Isogeometric shells admit high-accuracy, high-sparsity quadrature routines unavailable for traditional shells [92]. And finally, isogeometric techniques offer the potential of a single model suitable for both engineering design and analysis, reducing the time and expense associated with meshing.

Unfortunately, CAD models are not simply curvilinearly mapped rectangles, as are the B-spline and NURBS patches from which they emanate. Rather, CAD technologies piece B-spline and NURBS patches together to define the boundary of an intended object, a computational representation called a B-Rep. Midsurfaces of these models, called open B-Reps, are created analogously. For models with complicated geometry or topology, Boolean operations are typically employed to portray the intended shape by masking unwanted parts of the underlying spline patches [26, p. 304–307], [12, 58]. Aspects of this construction process are displayed in Figure 1. Visually, the results portray the intended design, but these Boolean (a.k.a. "trimming") operations hide what is often a complex computer representation (see Figure 2). Trimming breaks spline function continuity [26, p. 305], [58], complicates numerical integration [46, 60, 68], and requires weak coupling of subdomains [34, 71, 72, 75]. Because CAD software cannot exactly represent general trimming operations [44, 76], approximations are made that lead to tiny gaps and overlaps between surface edges that should be coincident [58, 77]. This leads to surfaces that are not "watertight." [58, 77].

In this paper, we propose a new framework for converting open midsurface CAD geometries into isogeometric analysis-suitable, trim-free B-Reps using discrete surface Ricci flow and metric optimization. In this framework, a trimmed CAD model is converted into an easy-to-compute, feature-aware surface triangulation with a topologically-constrained number of cone singularities (defined in Section 2). From there, the discrete surface Ricci energy is minimized to determine a flat metric on the surface with cone singularities: this metric can be thought of as an immersion of a cut version of the surface into the Euclidean plane, or a locally-bijective "parameterization." Subsequently, this parameteriztion is transformed into one that induces a quadrilateral layout on the surface. A quadrilateral layout can be thought of as a coarse quadrilateral partitioning of the surface that can be refined as much as desired while still guaranteeing a valid quadrilateral

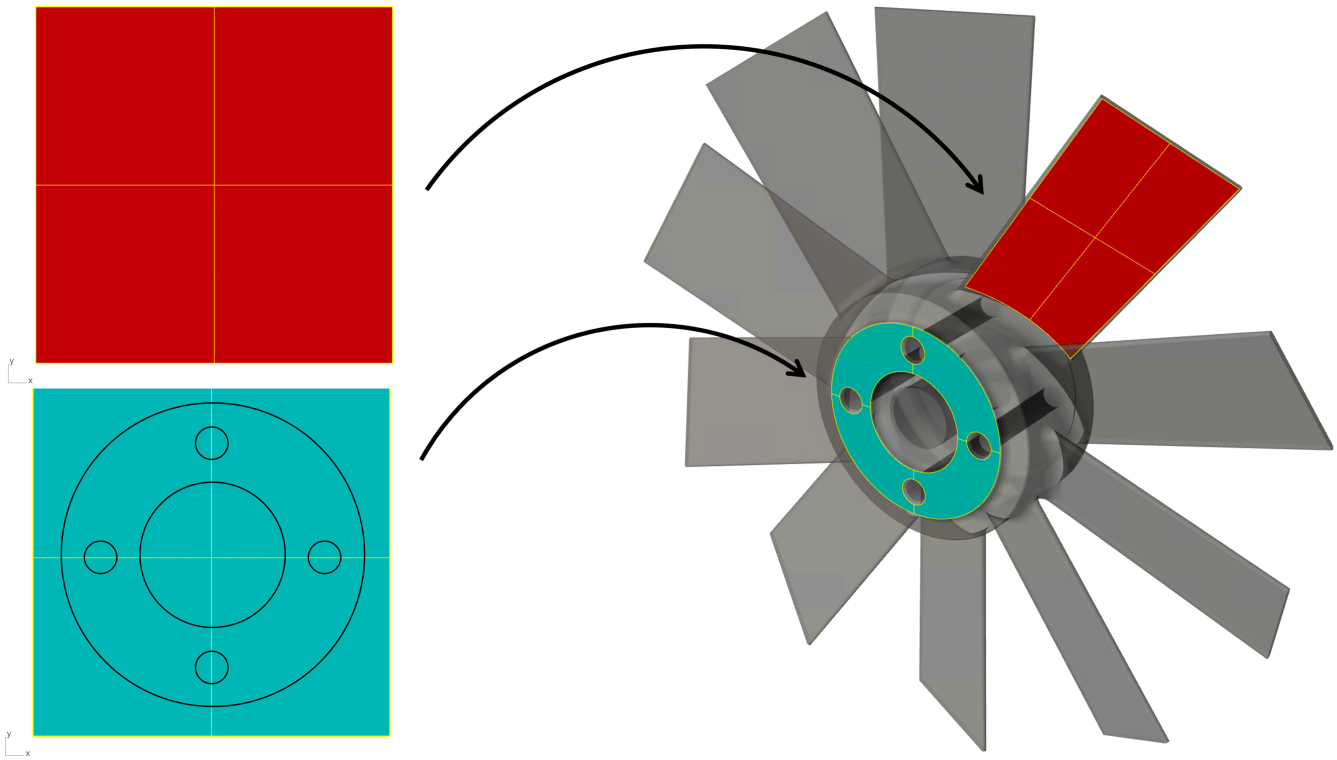

Figure 1: A typical B-Rep geometry will consist of a topological gluing of multiple B-spline and NURBS tensor product patches mapped into a spatial configuration. In the presence of complicated topology or geometry, trimming operations—which mask portions of the tensor product spline—are ubiquitous. These trimming operations, though useful in rapid design prototyping, impede the use of the B-Rep in engineering analysis. This particular B-Rep is a sample engine turbine from Rolls Royce.

refinement. Subsequently, the original CAD model is rebuilt using this computed layout as the skeleton for a set of quadrilateral watertight spline patches. Because this method employs a feature-aware triangulation for the quadrilateral parameterization computation, it works equally-well in converting a faceted mesh into a feature-aware smooth spline surface.

1.1. Prior Work

Two approaches have arisen to address the issues related to analysis of trimmed B-Rep models. The first, primarily driven by the analysis community, aims to address the issues of trimmed B-Reps by employing various generalizations of the classical cut cell method [46, 68, 75]. Here, cut elements are addressed using specialized integration techniques (see e.g. [46, 60, 68] and [9, p. 87-95]), numerical stabilization [19, 20, 57, 59], and weak enforcement of both connectivity and boundary constraints [34, 71, 72, 75]. This approach has seen significant progress of late [10, 34, 33], with recent works performing explicit dynamics computations on trimmed industrial B-Reps [51], but additional efforts are still needed to ensure robustness in the presence of poorly shaped trimmed parametric spaces.

The other primary approach aiming to address analysis of trimmed CAD models seeks to rebuild a trimmed B-Rep prior to use in analysis. Many methods have been developed to rebuild a trimmed

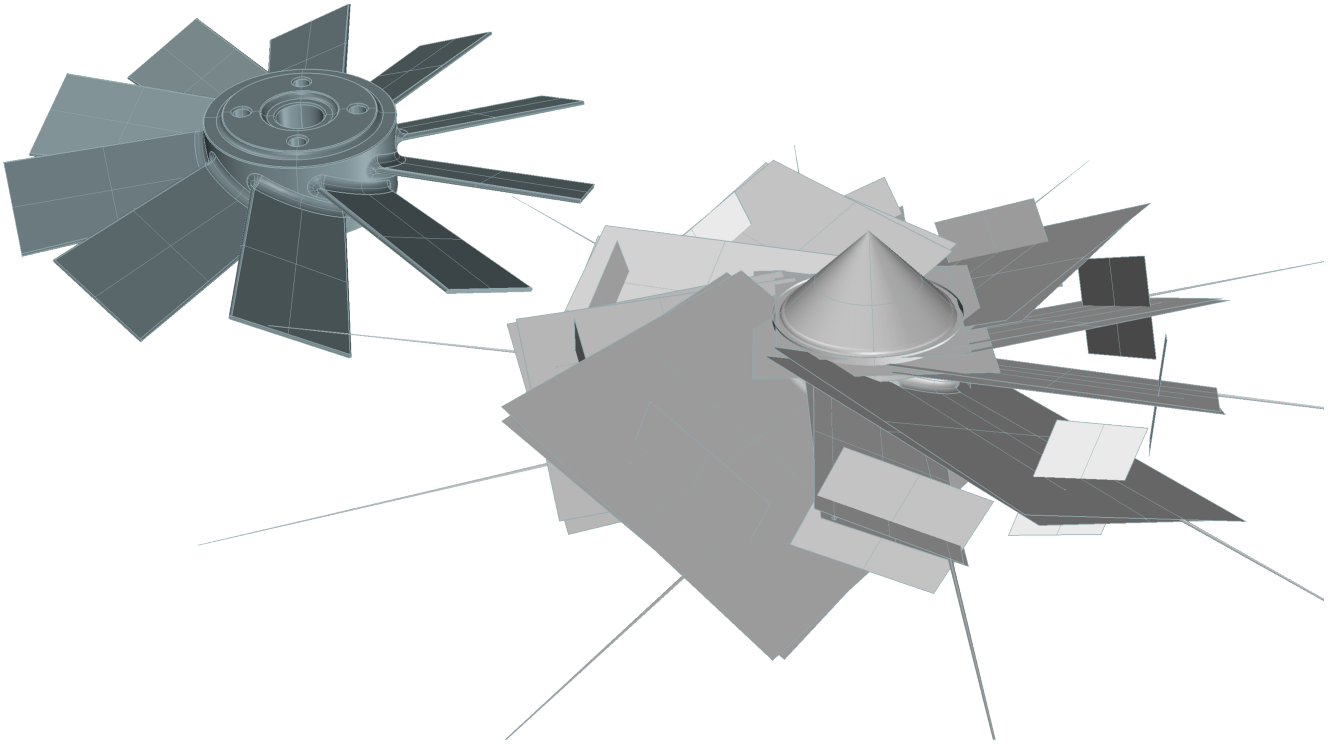

Figure 2: A trimmed B-Rep engine turbine from Rolls Royce (top-left) portrays an intended geometry, but the underlying computational representation visualized after removing trimming features reveals that the model is defined by a complicated data structure bearing very little resemblance to the intended geometry.

spline into a set of trim-free Bézier, B-spline, or NURBS patches by subdividing a trimmed patch's parametric domain into more regular shapes [66, 67, 77, 88]. These techniques work well when the original model already meets high quality criteria, but generally cannot perform well on models for which the designer prescribed a poor parametric spline definition. Unfortunately, many models of engineering interest (including that of Figure 2) may not meet the requisite quality criteria, and reconstruction using these techniques is difficult, and sometimes impossible. Alternatively, recent works aim to redefine the B-Rep's underlying parametric domain by computing a global reparameterization using an auxiliary feature-aware surface triangulation [7, 8, 13, 14, 22, 54]. Unlike typical analysis-suitable meshing methods that are predominantly well-structured quadrilaterals [5] and are labor-intensive to produce, the triangulations necessary for these reparameterizations can be unstructured and are easily-defined [81, 82, 83]. After computation of a quadrilateral-layout inducing reparameterization, splines are then fit to the computed layout. To date, many of these global reconstruction techniques have required significant user intervention [37, 87], require expensive mixed-integer optimization [7, 8, 14, 54, 56], are limited by the use of templates [1, 55] or certain types of singularities [30, 48, 49], or suffer from robustness issues [36]. Many are based on the frame field methods proposed in the computer graphics community [8, 47, 63, 69, 79], which frequently employ mixed-integer optimization [7, 8, 14, 54] and require heuristics to address errors introduced by the non-integrability of frame field vectors [24, 54, 79]. These methods generally cannot guarantee a locally-injective parameterization, meaning that some elements are either degenerate or

possess non-positive Jacobian.

1.2. Contributions

In this work, a global reparameterization technique is defined and employed in rebuilding both trimmed and faceted geometries of industrial relevance. Unlike many other global reparameterization methods, however, it does not require the use of mixed-integer optimization, and the resulting parameterization is guaranteed to have a well-defined inverse locally. Specifically, we make the following contributions.

- We define a set of generalized criteria on a triangulation that, if satisfied, yield a quadrilateral layout on the surface (Section 2).
- In Section 3.3, we present a set of partial differential equations that, in combination with Ricci flow, yield a quadrilateral layout-inducing parameterization on a faceted surface.
- We employ the technique in Section 4 to extract trim-free spline surfaces from the US Army's trimmed CAD model of the Unclassified DEVCOM Generic Hull vehicle [23] and from the National Crash Analysis Center's (NCAC's) finite element model of a 1996 Dodge Neon [28]. Extracted spline spaces include ones for which previous methods are known to fail (see [36] and [35, Appendix B]).
- Additionally, in Section 4 we demonstrate, using the isogeometric analysis capabilities in the commercial solver LS-DYNA, that the defined spline surfaces are suitable for use in isogeometric shell analysis.

The first contribution gives a general characterization that, if met, ensures that the computed parameterization on a triangulation defines a quadrilateral layout. The second provides an alternative approach for computing such a parameterization. The third and fourth demonstrate the potential of the proposed technique in creating isogeometric analysis-suitable shells from trimmed and faceted models. Finally, conclusions and future work are discussed in Section 5.

2. Definition of a Quadrilateral-Inducing Parameterization

This section is foundational but necessarily mathematical. It utilizes concepts from differential and algebraic topology and geometry with which many readers may not be familiar. We invite readers unfamiliar with this material to scrutinize figures in this section to attain at least a visual comprehension of the ideas.

Because the NURBS-based B-Rep is the predominant computational representation of CAD geometries, the target object of this work is a non-degenerate set of NURBS splines redefining the original geometry without any trimming. This could be thought of as a coarse, curvilinear quadrilateral mesh, called a quadrilateral layout, defined by a set of splines. This characterization emphasizes that each spline is a curvilinear quadrilateral, but leaves the global objective that the splines must fit together precisely along boundaries unaddressed. Such a local-to-global characterization is not amenable for computation, and so a different representation is necessary.

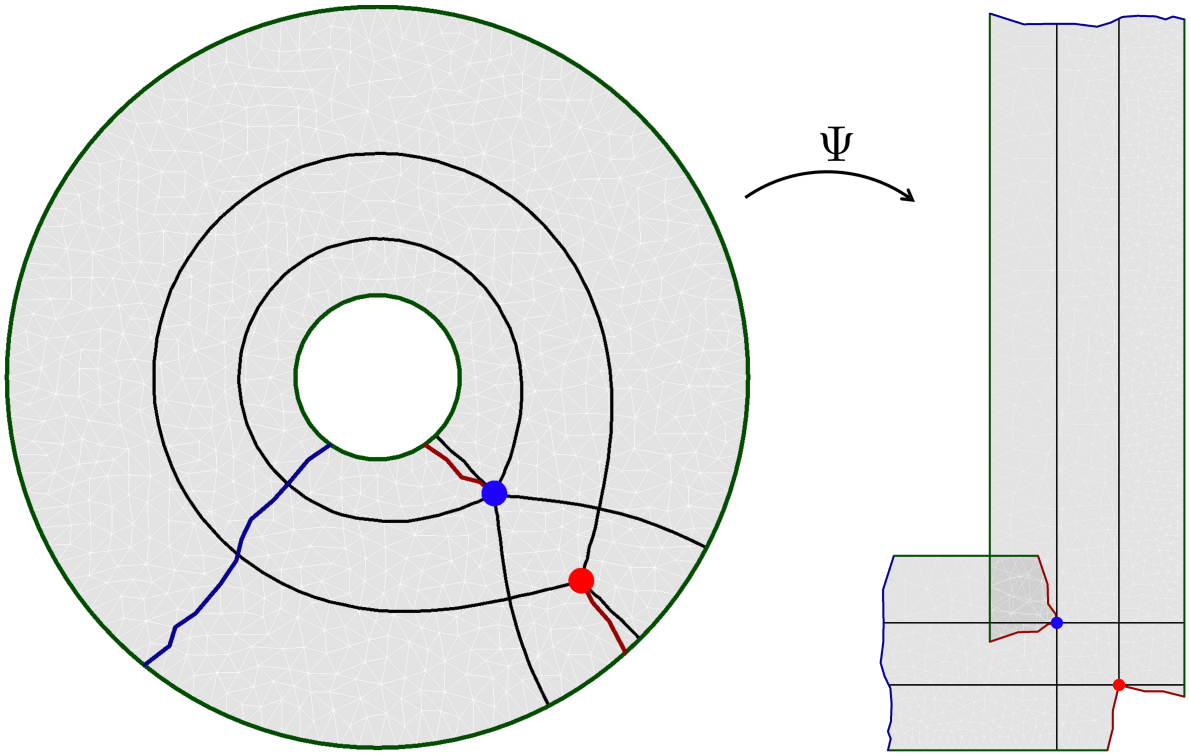

Figure 3: A contrived quadrilateral layout on an annulus (left) is induced by a mapping of the cut annulus into the Euclidean plane (right). Here, the point in blue is a cone singularities of valence five and the point in red is a cone singularity of valence three. Cuts to cone singularities are given in red, while cuts to make the bracket a topological disk are in blue. Boundary curves are in dark green, while non-boundary integral curves are given in black. The coordinate differentials, du and dv, when traced from singular points and pulled back from the Euclidean plane to the original surface, integrate into curvilinear arcs partitioning the surface into a set of quadrilaterals. These differentials are depicted as black lines of constant u and v coordinates in the immersion, and curvilinear black arcs when pulled back to the original surface.

Additionally, the trimmed spline spaces defining a CAD object also are not amenable for computation without weak coupling. As such, these geometries are converted to a feature-aware unstructured surface triangulation by, for example, triangulating individual parametric domains and mapping these triangulations using the surface mapping, taking care that nodes on on surface boundaries align appropriately. Given this triangulation, a global parameterization inducing a quadrilateral layout on the surface is defined by the following criteria of Definition 2.1. Two sample parameterizations satisfying all of these criteria are depicted on a contrived example for an annulus in Figure 3 and for a bracket of the DEVCOM vehicle in Figure 4. These criteria may best be understood pictorially, and the reader is invited to study Figures 5 through 9, in conjunction with Figures 3 and 4 for best comprehension.

Definition 2.1 (Quad Layout Immersion)**.** *Let S be an oriented,*[1] *triangulated surface with a prescribed set of singular points, P. Take G as a graph along edges of S making $S - G$ a (set*

[1]Surfaces of engineering interest are oriented. Non-orientable surfaces are objects like the Möbius band.

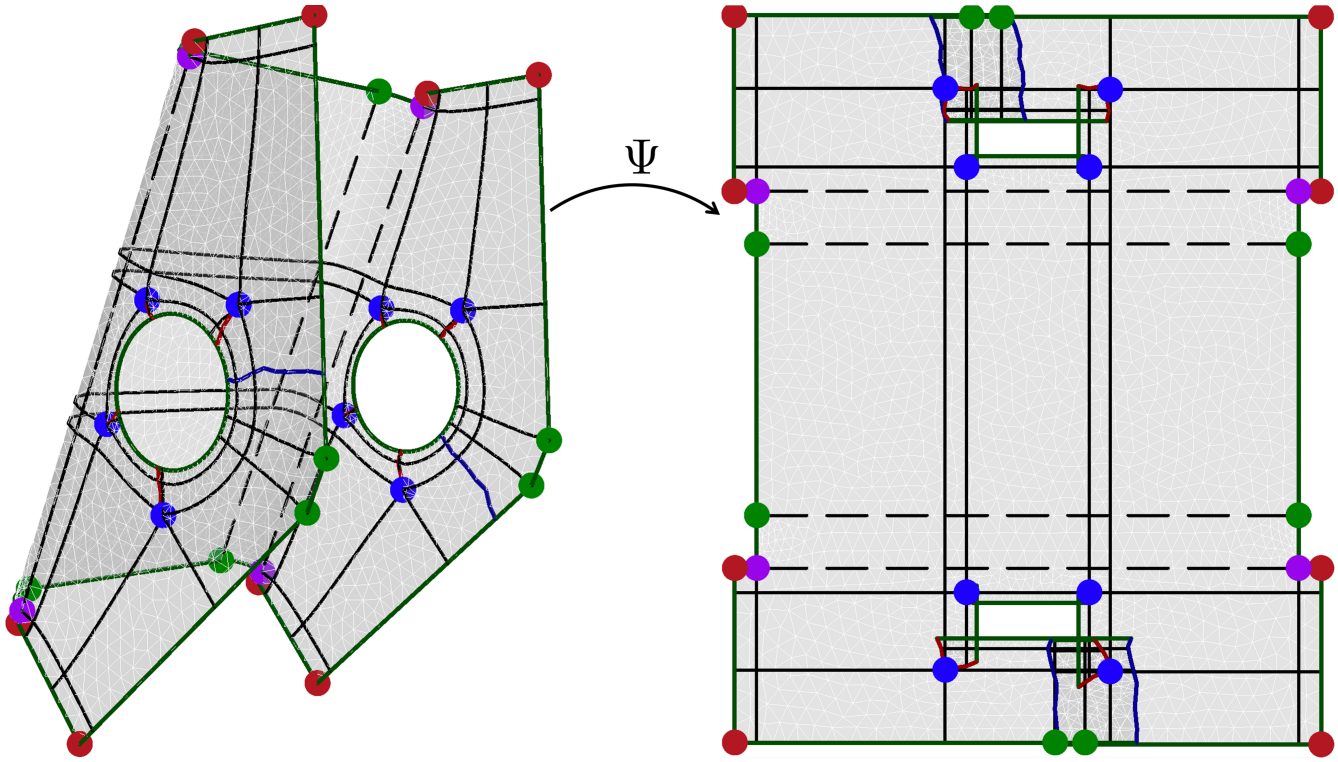

Figure 4: A quadrilateral layout on a bracket of the DEVCOM Generic Hull vehicle (left) is induced by a mapping of the cut bracket into the Euclidean plane (right). Here, points in blue are cone singularities of index -1 (valence five), points in red are boundary cones of index 1, and points in purple are boundary cones of index -1. Feature points of the model that are not cone singularities in the defined parameterization are displayed in green. Cuts to cone singularities are given in red, while cuts to make the bracket a topological disk are in blue. Feature curves to be preserved in the computed layout are in dashed black. The coordinate differentials, du and dv, when traced from singular points and pulled back from the Euclidean plane to the original surface, integrate into curvilinear arcs partitioning the surface into a set of quadrilaterals. These differentials are depicted as black lines of constant u and v coordinates in the immersion, and curvilinear black arcs when pulled back to the original surface.

of) topological disk(s) such that $P \subset G \cup \partial S$ (hereafter called a ***cutting graph****). With this representation, we assume that each edge through which G passes is represented as two edges in $S - G$, and similarly that vertices of S are split into multiple representations in $S - G$ (see Figure 5). Then a continuous map $\Psi : S - G \to \mathbb{R}^2$ that generates a quadrilateral layout (called a* ***quad layout immersion****) satisfies the following criteria.*

Q1 *Local injectivity: all but a discrete set of points (specifically, not singularities) have a neighborhood that is locally invertible (see Figure 6).*

Q2 *For each vertex v of the triangulation on S, take $U(v)$ to be the one-ring neighborhood (a.k.a. the closed star [38]) of v, with T a triangle of $U(v)$. For ease of notation, also write $U(v)$ as the set of triangles in the cut representation $S - G$, where now v may be cut, and is to be understood as the vertex incident to T after cutting. Define $\angle\big(v, \Psi(T)\big)$ as the inner angle of*

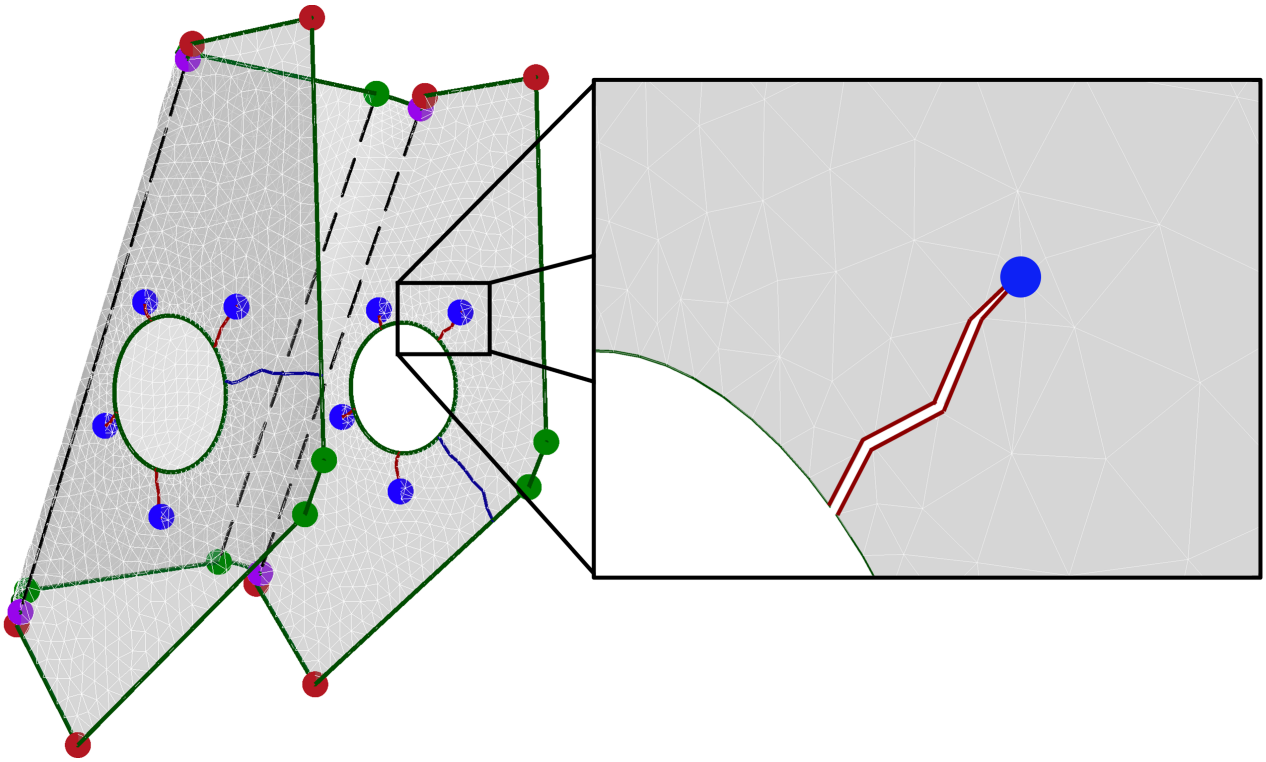

Figure 5: A bracket with computed singular and feature points is cut into a topological disk. Singular points are shown in red, purple, and blue, with those in red and purple representing boundary cone singularities of index 1 and -1, respectively, and blue points representing interior cone singularities of index -1 (valence five). Points in green are features of the bracket that are not chosen to be cone singularities in the parameterization. Cuts to singularities are depicted in red, while cuts to make the bracket a topological disk are in blue. Curves in dark green and dashed black are the surface boundary and features, respectively. Notice that each singular point is either in the cutting graph or the surface boundary. Edges in the cutting graph are represented twice in the cut surface, vertices that are cut through are multiply represented, and vertices at the termination of the cutting graph are singly represented.

$\Psi(T)$ *incident to vertex* $\Psi(v)$*. Then the following holds:*

$$\sum_{T \in U(v)} \angle\big(v, \Psi(T)\big) = \begin{cases} 2\pi & \text{if } v \notin P \text{ and } v \text{ is in the interior of } S \\ \pi & \text{if } v \notin P \text{ and } v \text{ is on the boundary of } S \\ \frac{k\pi}{2} & \text{for } k \in \mathbb{Z} \text{ if } v \in P \end{cases} \tag{1}$$

(See Figure 7 for an example in which $k = 5$*.) Furthermore, a discrete version of the Gauss-Bonnet theorem holds:*

$$\sum_{v \notin \partial S} \Big(2\pi - \sum_{T \in U(v)} \angle\big(v, \Psi(T)\big)\Big) + \sum_{v \in \partial S} \Big(\pi - \sum_{T \in U(v)} \angle\big(v, \Psi(T)\big)\Big) = 2\pi\chi(S), \tag{2}$$

where $\chi(S)$ *is the Euler characteristic of the surface.*[2]

[2]Recall that for a triangulated surface with V vertices, E edges, and F faces, $\chi(S) = V - E + F$, and is a

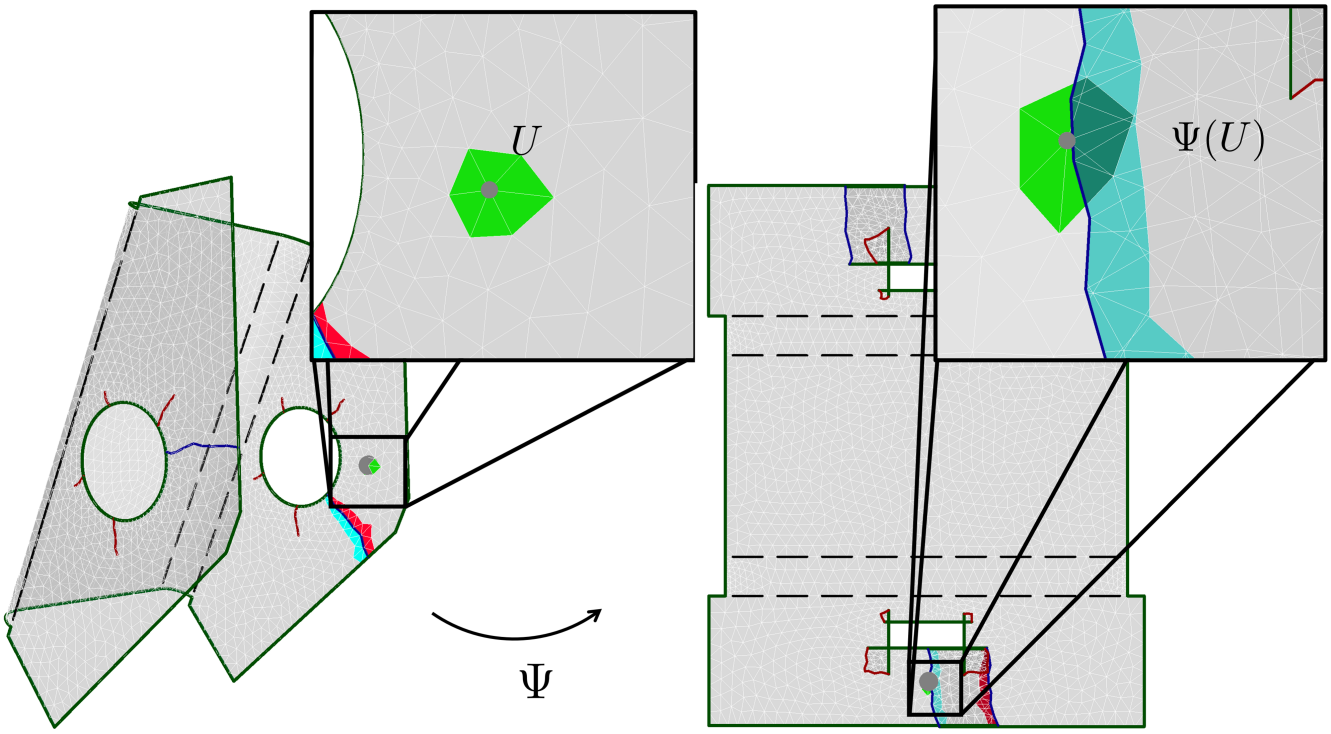

Figure 6: A bracket of the DEVCOM Generic Hull vehicle is triangulated, and the neighborhood of one of its vertices is shown in green and subsequently mapped via a quad layout immersion map, Ψ. Additionally, all triangular faces on the sides of a particular homological cut are represented in either red or cyan and similarly mapped. Under the immersion, the image of the bracket is no longer injective: for example, the map takes portions of the vertex's neighborhood to the same coordinate locations that are part of the cyan side of the cut. However, an inverse is well-defined locally throughout the surface, including for each of these colored neighborhoods.

Q3 *Each connected component of $\partial S - G$ is mapped by Ψ to a line with constant u or v coordinate (see Figure 8).*

Q4 *Let each arc of G be written by ω_i, be given an orientation, and be parameterized by arc length. Under $S - G, \omega_i$ is represented by ω_{+i} and ω_{-i} on the left and right side of ω_i, respectively, with parameterization consistent with ω_i. Then $\Psi\big(\omega_{-i}(t)\big) = \mathcal{T}\Big(\Psi\big(\omega_{+i}(t)\big)\Big)$ for $\mathcal{T} : \mathbb{R}^2 \to \mathbb{R}^2$ a translation and rotation by $\frac{k\pi}{2}, k \in \mathbb{Z}$ (see Figure 8).*

Q5 *Lines emanating from singularities under the immersion with constant u or v coordinate value, when pulled back to $S - G$, either*

1. *Terminate at a (possibly identical) singularity*
2. *Terminate transversely to the boundary*

topological invariant.

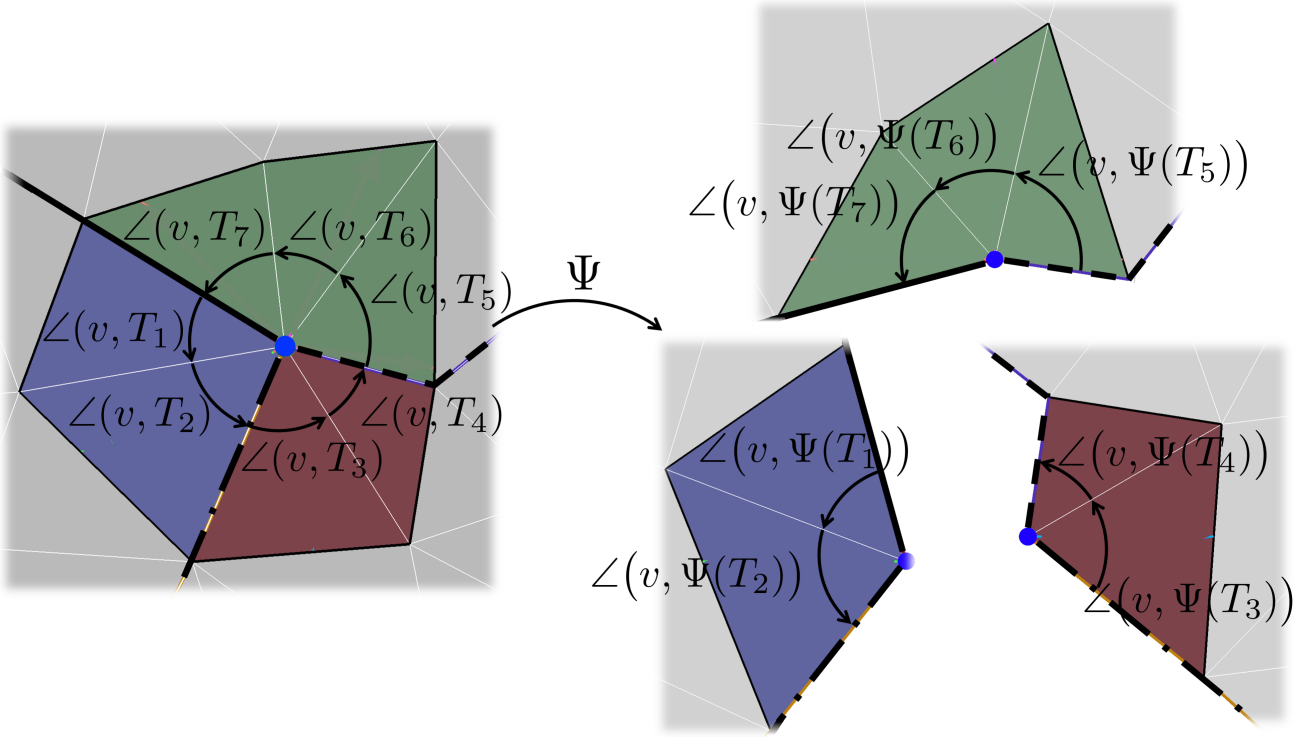

Figure 7: The cutting graph of a surface—shown as a solid line, a dashed line, and a dash-dot line—splits this singular point into three child vertices. Accordingly, the neighborhood is split into three different portions, shown in blue, dark green, and dark magenta. Under the immersion mapping, the sum of the interior angles of this vertex with its incident triangles is $\frac{5\pi}{2}$, making the point a cone singularity of index -1 (i.e. valence five).

> *3. Are transverse to the cutting graph G*
>
> *In the final case, the line is continued inductively across the cut using the transformation $\mathcal{T}$ prescribed in Item **Q4** (see Figure 9). All such sets of lines are finite, i.e. they achieve Item (1) or (2) twice.*[3] *The set of these curves emanating from singularites are frequently called **separatrices**.*

*Furthermore, if these conditions hold, then any curve generated as in Item **Q5** at any point on the surface will be finite (either periodic, part of the separatrices, or terminating transverse to two boundaries). These curves are called **isocontours** or **integral curves**.*

These criteria are presented in the smooth setting in [80]. The prescribed set of vertices P are called **cone singularities**. If the set of cone singularities satisfies Equation 2, it is said that the set is "admissible." Property **Q3** is referred to as the boundary-alignment constraint. For frame field-based parameterization methods, Property **Q1** is referred to as integrability of a frame field

[3] In the case that S is an annulus with no singularities or a torus with no singularities, the same holds after artificially calling an arbitrary regular point the surface's only singularity and proceeding as before.

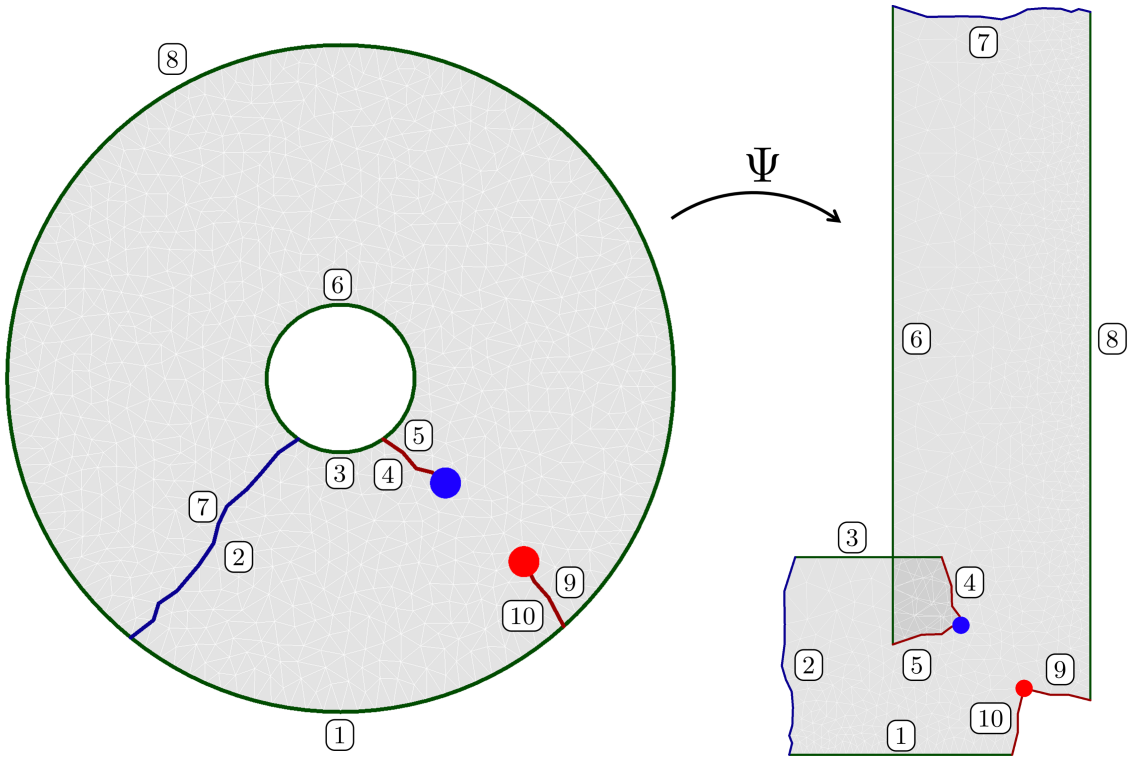

Figure 8: A cut version of an annulus with a valence three (red) and a valence five (blue) singularity has subdomains of its boundary labeled. Because the cut surface is a topological disk, members of the cutting graph are also included. Under the quadrilateral layout inducing parameterization, Ψ, curves 1 and 3 are mapped to lines of constant v coordinate and curves 6 and 8 are mapped to lines of constant u coordinate. After a translation, curve 2 rotated by $\frac{\pi}{2}$ radians counter-clockwise (CCW) aligns with curve 7, and curve 4 matches curve 5 after rotation by $\frac{\pi}{2}$ radians CCW, and curve 9 matches curve 10 after rotation by $\frac{3\pi}{2}$ radians CCW.

[21]. Properties **Q1**, **Q2**, and **Q4** together define a so-called "seamless surface parameterization" [15]. Property **Q5** is frequently satisfied by obeying integer-grid constraints [7, 8, 14, 24, 54]. Alternative characterizations of a quadrilateral layout as a special Riemannian metric on a surface and as a meromorphic quartic differential are given in [17] and [50, 91], respectively.

In a spline parameterization, the aforementioned cone singularities are referred to as "extraordinary points" or "star points," particularly when located in the interior of the surface. The **valence** of a spline node is defined as the number of spline edges emanating from the node. Extraordinary points correspond to boundary nodes whose valence is not three, or interior nodes with valence not equal to four. Because extraordinary points are not commonly defined on boundaries and because these cone singularities live on the surface triangulation, we define the **index** of a vertex, v, on the surface triangulation as

$$I(v) = \begin{cases} \frac{2}{\pi}\left(2\pi - \sum_{T \in U(v)} \angle\big(v, \Psi(T)\big)\right) & \text{if } v \notin \partial S \\ \frac{2}{\pi}\left(\pi - \sum_{T \in U(v)} \angle\big(v, \Psi(T)\big)\right) & \text{if } v \in \partial S. \end{cases} \tag{3}$$

Accompanying the index, the following Gauss-Bonnet condition holds, which is equivalent to that

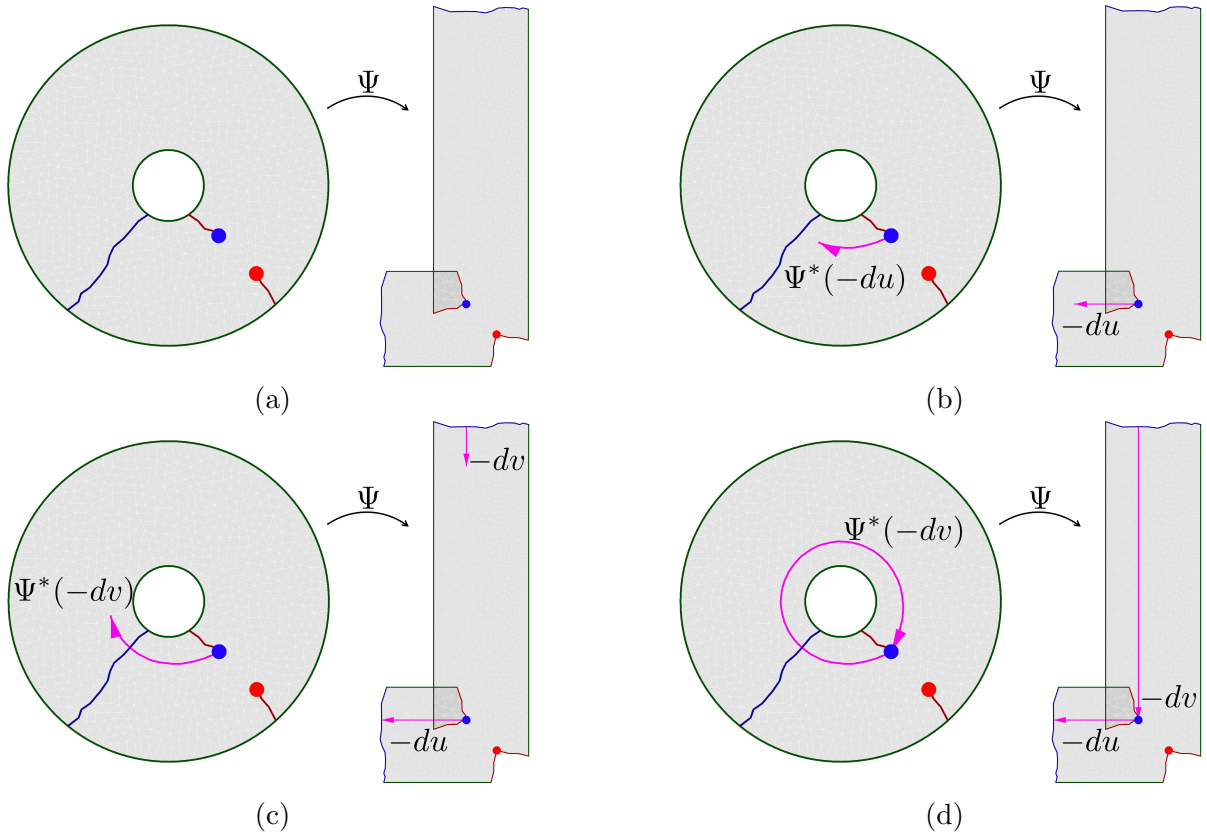

Figure 9: An integral curve emanating from a singular curve in the $-du$ coordinate direction is extracted (a line of constant v in the immersion). On the right of each subfigure is the integral curve under the quad layout immersion, Ψ, while on the left the integral curve of the pullback, Ψ^*, of the coordinate function differential into the spatial domain is shown. After reaching the cutting graph, the integral curve is continued in the $-dv$ coordinate direction on the opposite side of the cut: the direction and location for continued integration is prescribed by Property **Q4**, and will generate a continuous curve in the spatial domain. This particular integral curve terminates when it returns to the singular point from which it began.

in Property **Q2**:

$$\sum_{v \in S} I(v) = 4\chi(S). \tag{4}$$

The index is an integer-valued function defining the discrete contribution of a point to the surface's total curvature. Regular points have index zero, while cone singularities will have non-zero values. A cone singularity v corresponds to a point of valence $4 - I(v)$ if v is in the interior of S, and a point of valence $3 - I(v)$ if it is on the boundary.

Definition 2.1, though long and a bit arduous, provides a global, computationally-amenable framework for defining a quadrilateral surface parameterization. Given this characterization, the following section defines a set of partial differential equations used to produce such a parameterization.

3. Computation

Given the global recharacterization of a quadrilateral layout as a special type of immersion mapping into the Euclidean plane, as described in Definition 2.1, we proceed to define how to realize this characterization. Figure 10 walks through this reconstruction process for a contrived yet instructive example of a plate with a hole and a single feature curve, and will be referred to throughout this section.

3.1. Selection of Singular Points

After having extracted a feature-aware triangulation of the B-Rep (or having subdivided a faceted mesh into a triangulation), a set of singular points must be defined that obey the Gauss-Bonnet condition of Equation 2 (or equivalently Equation 4). For surfaces, this discrete Gauss-Bonnet condition is analogous to the discrete Poincaré-Hopf theorem for frame fields presented in [47, 70].

For this work, we employ the frame field method of [36], which combines aspects of [47] and [63], to automatically place a set of cone singularities. When the prescribed mesh is sufficiently smooth, the results of [47] guarantee that an admissible set of cones is prescribed. However, if the mesh lacks smoothness, has a number of features, or requires prescription of extraordinary points not of valence three or five, manual adjustment may need to be performed. Additionally, the engineer should check to see if the cones are placed in geometrically meaningful locations; if not, the problematic cones should be repositioned for a higher-quality spline reconstruction. For instance, Figure 11 (a) shows cone singularities automatically computed using the frame field method of [36]: while many singularities are well-placed, some cluster in a way that would benefit from singularity merger, and additional singularities must be introduced because the mesh lacks smoothness necessary to guarantee the Gauss-Bonnet condition of [47]. Instead, these automatically computed singularity positions for a Dodge Neon firewall are manually adjusted to satisfy Gauss-Bonnet, for better positioning, and to combine clustered low-valence singularities into higher-valence ones. All cones of the reference example, Figure 10, were placed manually. Better placement of these cones in an automatic or semi-automatic manner for featured geometries is a topic for future research.

3.2. Discrete Surface Ricci Flow

After selection of an admissible set of cone singularities (obeying the Gauss-Bonnet condition of Equation 2), a flat metric on the surface with cone singularities is computed using discrete surface Ricci Flow [18, 29, 31, 42, 90]. A thorough discussion of discrete surface Ricci flow is presented in [42], with a generalization to less regular meshes given in [90]. Here we briefly review the basic concepts related to this flow.

3.2.1. Ricci Computation

Every surface, S, embedded in $\mathbb{R}^3$ with a triangulation, $\mathfrak{T}$, inherits the Riemannian metric of $\mathbb{R}^3$. Here, each face T_{ijk} with vertices v_i, v_j, v_k inherits lengths from Euclidean space and angles obeying the typical law of cosines:

$$\ell_{ij}^2 = \ell_{jk}^2 + \ell_{ki}^2 - 2\ell_{jk}\ell_{ki}\cos\left(\angle(v_k, T_{ijk})\right) \tag{5}$$

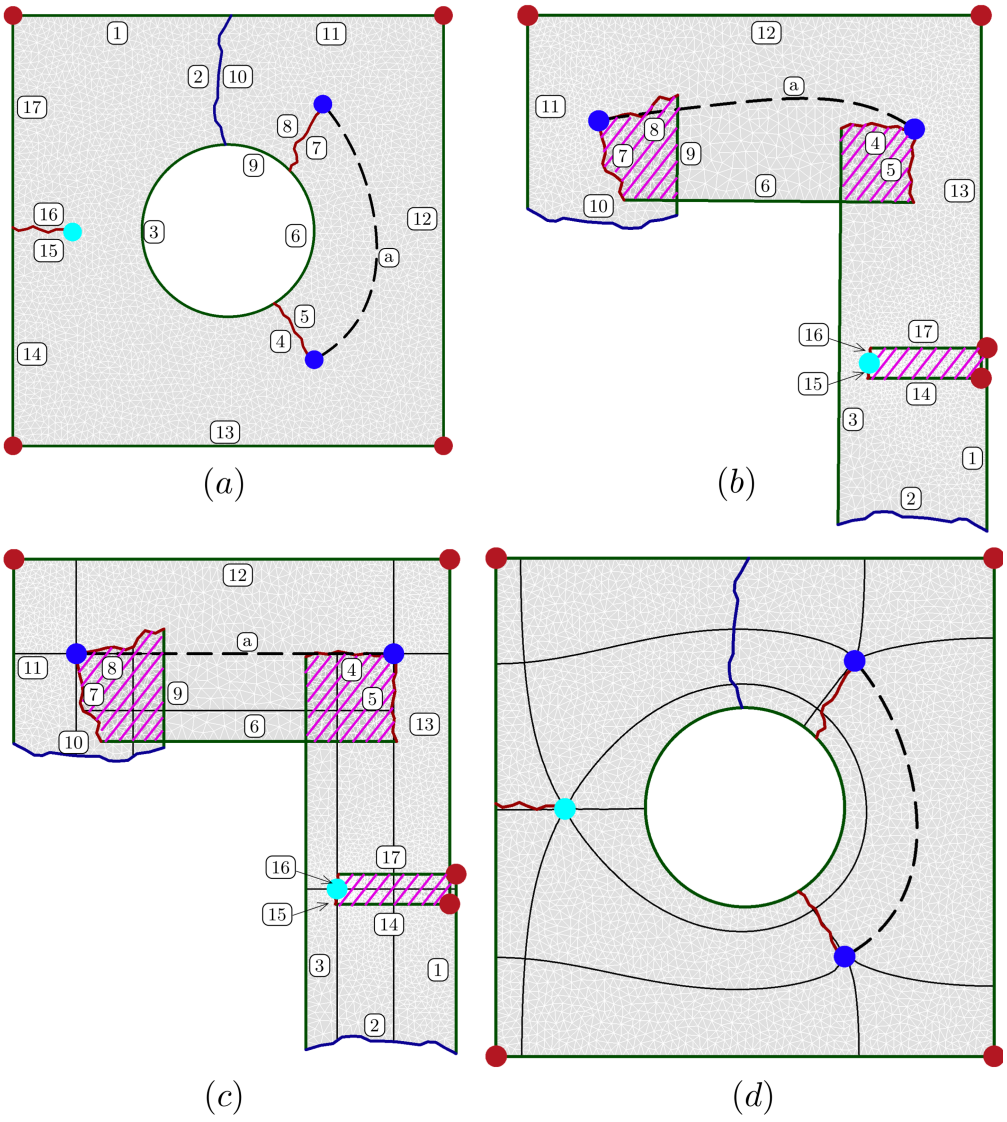

Figure 10: The layout reconstruction process is shown for a contrived, but instructive example. In (a), a set of cone singularities are prescribed, with two interior cones of index -1 (valence 5), one interior cone of index -2 (valence 6), and four boundary cones of index 1. Cuts are made to each cone and to make the surface a topological disk, with edges of the disk labeled in clockwise manner; a feature curve is also shown as a dashed line and labeled using an "a." In (b), the surface is immersed into the plane based on the computation of discrete surface Ricci flow. This immersion does not induce a feature-aligned quadrilateral layout because the feature curve is not a line of constant u or v coordinate and because the boundary curves on the reentrant corners of the L-shaped immersion are also not lines of u or v coordinates. This parameterization is minimized against a quadrilateral layout-inducing energy to yield (c), an immersion that induces the quadrilateral layout of (d). In addition to the boundary curves and the feature curve "a," the black lines of (c) and (d) are integral curves from the singular points yielding the quadrilateral layout. Regions of magenta hatching are locations in which the immersion maps, though locally invertible, are not globally invertible.

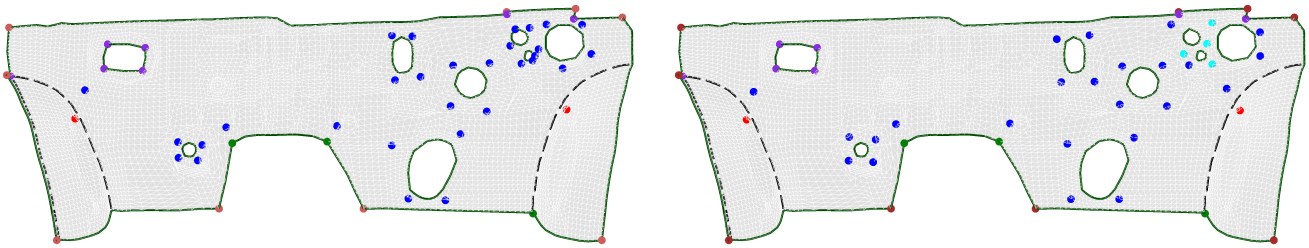

(a) Automatically Computed Singularities (b) Manually Adjusted Singularities

Figure 11: On the left, singularities are automatically computed using [36], which combines the theory from [47] and [63]. Because of the high clustering of cone singularities in this configuration, singularities were manually modified to combine valence five singularities (blue) into valence six singularities (cyan) in the regions of high clustering (right). Note that the automatically-computed locations clarify potential positions for the manually-adjusted configuration.

where ℓ_{ij} is the length of the edge between v_i and v_j, and $\angle(v_k, T_{ijk})$ is the interior angle of triangle T_{ijk} at vertex v_k. Take $\mathfrak{V}$ as the set of all vertices in the surface triangulation.

Defining the discrete Gaussian curvature at a vertex on the surface to be

$$K_i \equiv K(v_i) = \begin{cases} 2\pi - \sum_{T \in \mathfrak{T}, v_i \in T} \angle(v_i, T) & \text{if } v_i \notin \partial S \\ \pi - \sum_{T \in \mathfrak{T}, v_i \in T} \angle(v_i, T) & \text{if } v_i \in \partial S, \end{cases} \tag{6}$$

then the following discrete Gauss-Bonnet theorem holds [32, p. 252–253]:

$$\sum_{v_i \in \mathfrak{V}} K_i = 2\pi\chi(S). \tag{7}$$

From here, a parameter γ_i is selected for each v_i : this represents the length of the radius of a circle about v_i for a discrete circle-packing metric on the surface [18, 42, 90]. Taking a conformal factor

$$u_i = \log(\gamma_i) \tag{8}$$

(with potential choices of u_i given in [42, 90]), discrete Euclidean surface Ricci flow is governed by the following nonlinear, partial differential equation:

$$\frac{\partial u_i}{\partial t} = \bar{K}_i - K_i, \tag{9}$$

where $\bar{K}_i$ is the input target curvature. Recall that in this instance, $\bar{K}_i$ will be zero for all non-singular points and predefined based on the type of cone singularity for all other points.

Alternatively, discrete surface Ricci flow can be recast as the unique minimizer of the following convex energy,

$$E(u) = \int_0^u \sum_{i=1}^{n} (\bar{K}_i - K_i), \tag{10}$$

where n is the number of vertices in $\mathfrak{V}$. Newton-like methods can be used to efficiently minimize this energy [42, 90].

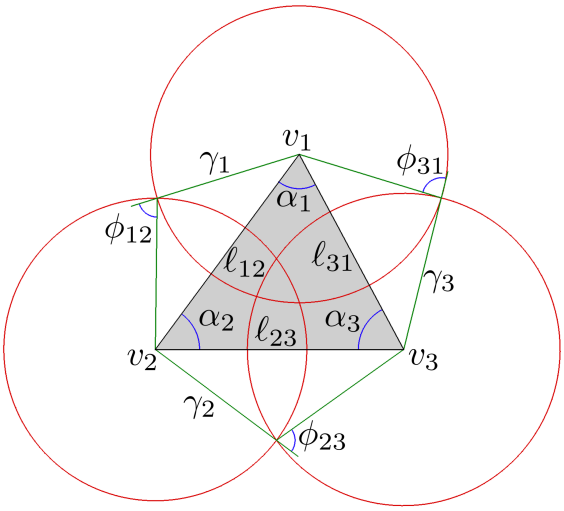

Figure 12: After minimizing the discrete Ricci flow energy, the cut surface with flat metric can be isometrically immersed into the Euclidean plane using the law of cosines of Equation 11 in conjunction with the lengths and angles depicted in this figure.

3.2.2. Metric Immersion

Upon solving for each u_i by minimizing Equation 10, the surface has a flat metric with cone singularities. This is converted to an immersion mapping into the two-dimensional Euclidean plane by transforming the computed conformal factors to circle radii (using Equation 8), and using a fixed, conformal edge weight $\cos(\phi_{ij})$ in conjunction with the following law of cosines (see Figure 12):

$$\ell_{ij}^2 = \gamma_i^2 + \gamma_j^2 + 2\gamma_i\gamma_j \cos(\phi_{ij}). \tag{11}$$

After one surface triangle, T, has been immersed into the plane with arbitrary rotation, neighboring triangles are then mapped into the plane and glued to an edge of T in a similar manner. Proceeding until all surface faces have been visited once will effectively define a map from a cut version of the surface into the Euclidean plane. For the sake of computational simplicity, it is often preferable that these cuts go to, but not through singular points (meaning that a small neighborhood of every singular point is a single connected component under the cutting operation). Recall the set of these cuts, G, is the cutting graph.

For genus zero surfaces with boundary, the surface can be immersed into the Euclidean plane using this metric to satisfy Properties **Q1**, **Q2**, and **Q4** of Definition 2.1 [17], leaving only boundary-alignment, feature alignment, and finite-length integral curves to be addressed. More general surfaces will of necessity only satisfy Properties **Q1** and **Q2**. Because we always assume that the surfaces here are open shells (so genus zero with boundaries), we additionally assume that there is an edge in the boundary of S that, under this immersion mapping, has constant u or v coordinate; if not, perform a rotation to make this true.

Figure 10 (b) depicts the immersion of a cut version of a plate with a hole—Subfigure (a)—into the Euclidean plane based on surface Ricci flow. Here, cuts to cone singularities are shown in red (edges $4, 5, 7, 8, 15$ and 16), while cuts to make the surface a topological disk are given by edges in blue (edges 2 and 10). This computed map is locally injective, but does not induce a

feature-aligned quadrilateral layout because the feature curve, curve "a," is not constant in either u or v coordinate. Furthermore, the edge boundaries on the reentrant corners of the L-shaped immersion are not actually constant in u or v, though they are nearly so. This immersion will be transformed into the quadrilateral layout-inducing parameterization of Figure 10 (c) using the following techniques.

3.3. Minimization against a Layout-Inducing Energy

Having parameterized the surface by immersing it into the plane, it now remains to transform this parameterization into one that induces a quadrilateral layout, and thus meets all of the requirements of Definition 2.1.

Because all of Definition 2.1 must be enforced, there will accordingly be a variety of constraints on surface subdomains. These subdomains will be written using the following symbols: $\Gamma_u, \Gamma_v, \Gamma_u^{\text{feature}}, \Gamma_v^{\text{feature}}$, and $\Gamma_{\text{Hol}_k}, k \in \{0, 1, 2, 3\}$. Each of these constrained subdomains is geometric in nature and can easily be visualized: without this appeal to geometry, however, the notation can be heavy. To alleviate this issue, we first present these subdomains on our reference example, Figure 10, prior to defining the minimization problem and the definition of these symbols. It may be helpful to refer to Figure 10 throughout this section. In this figure, boundary curves curves $1, 3, 9, 11$, and 13 comprise the set Γ_u, boundary curves $6, 12, 14$, and 17 comprise Γ_v, and the feature curve "a" defines $\Gamma_v^{\text{feature}}$. The edges of 4 and 5 should be related to one another via Γ_{Hol_1} or Γ_{Hol_3} (depending on which side is used as reference). Similarly, edges 7 and 8 should be related to one another via Γ_{Hol_1} or Γ_{Hol_3}, edges 2 and 10 should be related using Γ_{Hol_2}, and edges 15 and 16 should be related using Γ_{Hol_2}. Both $\Gamma_u^{\text{feature}}$ and Γ_{Hol_0} are empty.

Additionally, note that the Ricci parameterization (Figure 10 (b)) and the quadrilateral-layout inducing parameterization (Figure 10 (c)) both have regions that lie on top of one another, shown with magenta hatching—particularly near the interior cone singularities. Nonetheless, both parameterizations are locally invertible, non-degenerate, and preserve the surface orientation with the mapping. As a result, non-singular locations in the domain have a well-defined inverse mapping with positive Jacobian.

Having established a point of reference for notation, we now proceed defining the minimization problem with its relevant subdomains in the general setting. Let Ω be the domain of the cut surface, $S - G$, and $\psi_R : \Omega \to \mathbb{R}^2$ be the immersion mapping defined by Ricci flow. Take

$$\mathfrak{F} = \{\varphi : \Omega \to \mathbb{R}^2, \varphi \in C^0(\Omega), \varphi \text{ locally invertible}\}. \tag{12}$$

This defines the set of continuous maps that have a well-defined inverse map. For functions in this family, take $u : \Omega \to \mathbb{R}$ as the parametric u coordinate of the function, $v : \Omega \to \mathbb{R}$ as the parametric v coordinate. Call a vertex, edge, or face of Ω the child of some parent vertex, edge, or face in S if both the child and parent occupy the same space in $\mathbb{R}^3$. Notice that for edges in G, there will be two children edges of Ω corresponding to a single edge of S, as seen in Figure 5.

Take e_{ij} as an edge in Ω between vertices v_i and v_j in which $|u(v_i) - u(v_j)| \leq |v(v_i) - v(v_j)|$ and e_{ij} has a parent in ∂S. Define the set of all such edges as Γ_u, and take the all edges in Ω whose parents are also in ∂S but not belonging to Γ_u as Γ_v. Let feature curves of S (and thus of Ω) similarly be classified as members of $\Gamma_u^{\text{feature}}$ or $\Gamma_v^{\text{feature}}$ based on whether the flux across them is greater in v or in u, respectively.

Similarly, let β be a continuous path in $G \subset S$ with start and end points that are one of the following

- singular points,
- transverse to a boundary of S, or
- do not have two children in Ω.

Take each interior vertex of the path to have two children in Ω. Thus, each path β will have two continuous children paths in Ω, and each child path will have exactly one child of edges contained in $\beta \subset G$. Define γ as one of these children, ω as the other, and take $\tau(\gamma)$ as the unique translation taking one child vertex of γ to its corresponding sibling in ω, v_ω. Define $R_{\hat{k}}, \hat{k} \in \{0, 1, 2, 3\}$ as a rotation by $\frac{\hat{k}\pi}{2}$ radians about v_ω. Take k to be number for which the rotation by R_k minimizes the deviation between ω and $R_k\big(\tau(\gamma)\big)$. Set Γ_{Hol_k} to be the set of all such β paths in which the rotation R_k is used.

Lastly, assume an input set of path connectivity constraints to be enforced between points p, q in the parameterization—typically between singular or feature points that should be connected by an integral curve. These path constraints should be defined in the homotopy class of $S - P$ that they are intended to follow, though the precise path is not important. The paths may be cut by G, and the primary direction of each subcurve under the parameterization mapping may differ across cuts; these subcurves must be consistently oriented to form a continuous, smooth curve on the branched covering space of the surface [43] defining the quadrilateral layout. Call the set of such constraints Γ_{topo}. Note that each subcurve γ_i of the topologically constrained curve $\gamma_1 \cdot (\dots) \cdot \gamma_\ell$ will be bounded by G, p, or q.

Based on this information, the parameterization sought minimizes the following energy.

Find $\psi \in \mathfrak{F}$ such that

$$\psi = \min_{\varphi \in \mathfrak{F}} \sum_{j=1}^{5} \lambda_j E_j \tag{13}$$

with

$$E_1(\varphi) = \int_\Omega ||J||_F^2 + ||J^{-1}||_F^2 d\Omega \tag{14}$$

$$E_2(\varphi) = \int_{\Gamma_u} \Big(\frac{\partial u}{\partial s}\Big)^2 d\Gamma + \int_{\Gamma_v} \Big(\frac{\partial v}{\partial s}\Big)^2 d\Gamma \tag{15}$$

$$E_3(\varphi) = \int_{\Gamma_u^{\text{feature}}} \Big(\frac{\partial u}{\partial s}\Big)^2 d\Gamma + \int_{\Gamma_v^{\text{feature}}} \Big(\frac{\partial v}{\partial s}\Big)^2 d\Gamma \tag{16}$$

$$E_4(\varphi)) = \sum_{k=0}^{3} \sum_{(\beta \in \Gamma_{\text{Hol}_k})} \int_\beta \Big(\frac{\partial \varphi_+}{\partial s} - R_k^{-1}\big(\frac{\partial \varphi_-}{\partial s}\big)\Big) \cdot \Big(\frac{\partial \varphi_+}{\partial s} - R_k^{-1}\big(\frac{\partial \varphi_-}{\partial s}\big)\Big) \partial\Gamma \tag{17}$$

$$E_5(\varphi) = \sum_{\gamma_1 \cdot (\dots) \cdot \gamma_\ell \in \Gamma_{\text{topo}}} \Big(\sum_{j=1}^{\ell} \int_{\gamma_j} \frac{\partial \varphi_{j_k}}{ds} d\Gamma\Big)^2 \tag{18}$$

$$= \sum_{\gamma_1 \cdot (\dots) \cdot \gamma_\ell \Gamma_{\text{topo}}} \Big(\sum_{j=1}^{\ell} \varphi_{j_k}\big(\gamma_j(1)\big) - \varphi_{j_k}\big(\gamma_j(0)\big)\Big)^2. \tag{19}$$

Here, J is the Jacobian transformation from Ω to $\mathbb{R}$ (local to each triangle), with $||J||_F$ representing the Frobenius norm, and φ_{j_k} is the constrained direction and orientation ($k = 0$ is $+u$, $k = 1$ is $+v$, $k = 2$ is $-u$ and $k = 3$ is $-v$) for the subcurve γ_j. The first energy aims for a smooth deformation ($||J||_F^2$ term) while also ensuring that local injectivity is preserved ($||J^{-1}||_F^2$ term), and is called the symmetric Dirichlet energy [85]. It preserves Property **Q1** of Definition 2.1. The next energy ensures boundary-alignment constraints, and helps satisfy Property **Q3**. Energy E_3 gives control over feature alignment, and ensures that features of the triangulation (preserved from the B-Rep) are preserved. Next, energy E_4 enforces Properties **Q2** and **Q4**. Finally, energy E_5 can be used to satisfy Property **Q5**.

The above energy is non-linear with penalty terms, and can be minimized using Newton-like iteration. Note that the initial parameterization guess, ψ_R, will not exactly satisfy many of the necessary constraints, so constraints transforming it into a quadrilateral layout must be enforced weakly. Because a Nitsche formulation will not generally yield the exact satisfaction of these constraints (which is necessary for the parameterization to yield a layout, as in Definition 2.1), we instead opt for iteratively solving using a penalty method. Here, as $\lambda_j \to \infty$ for $j = 2, \ldots, 5$ the parameterization converges to enforcing exact constraint satisfaction. For all operations, $\lambda_1 = 1$ is selected to preserve local injectivity, while the other penalty terms are gradually increased. This minimization problem can be solved efficiently using techniques such as [52, 65, 84]. It is often valuable to switch J between referencing the Euclidean geometry of the surface and the Ricci metric of the surface to extract the solutions of subsequent minimizations with increased lambda values from local minima.

4. Results

We demonstrate the efficacy of the proposed framework by reconstructing both trimmed and faceted models of industrial vehicles into trim-free spline representations suitable for isogeometric analysis. Here, integral lines emanating from singular points, from feature vertices, and along boundaries are extracted from the surface triangulation's parameterization, yielding a feature-aware quadrilateral partitioning of the surface. From here, cubic spline curves are fit using a least squares approximation of the integral lines. Lastly, surfaces are extracted using Coons patch interpolation. As such, all B-Reps have C^0 continuity between adjacent patches, and at least C^2 continuity in their interiors.

4.1. DEVCOM Generic Hull

The US Army's DEVCOM Generic Hull vehicle was created in an initiative to involve academia and industry in the research of under-vehicle blast phenomena without the challenges posed by operating on classified material [23]. The entire vehicle is comprised of an outer hull with various structural beams and pillars composing the structural frame. The midsurfaces of a structural bracket and two beams were extracted from the frame for reconstruction, shown in reference to the rest of the vehicle's primary structural members in Figure 13.

The bracket, which has been reconstructed in [36] using a global frame field-based approach, is shown in Figure 14. Here, it is shown in its trimmed form, its untrimmed form, and its reconstructed form using the present method. Additionally, its form after reconstruction using the method of [36] is presented for reference. While both the layout computed using Ricci flow with metric optimization

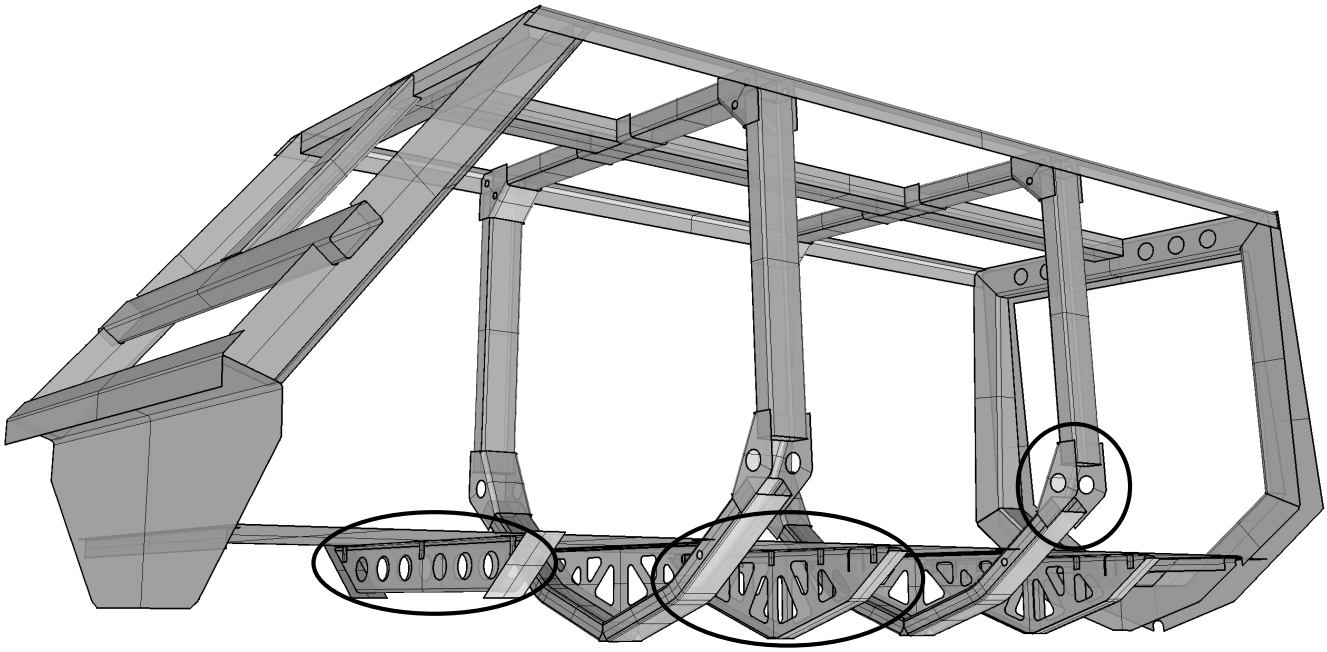

Figure 13: Three reconstructed parts of the DEVCOM Generic Hull vehicle [23]—two support beams and a bracket of a structural pillar—are shown in the context of the primary support members for the vehicle. All surfaces in this representation are trimmed.

and the layout of [36] have singular points in the same locations, the frame field layout produces integral curves that are more geodesic on the original geometry, while the proposed method is more biased to the geodesic curvature of the nearby boundary. As seen in Figure 15, both methods yield splines whose Jacobians are comparable.

Both rebuilt beams are also depicted with their trimmed and untrimmed representations (see Figures 16 and 17). However, the frame field method of [36] failed to produce a valid parameterization for these models, so the layouts produced from this work are not compared against an alternative global reparameterization technique.

For analysis, each bicubic Bézier patch was uniformly refined into a bicubic NURBS patch with 8×8 Bézier patches each using single-multiplicity knot insertion. Implicit modal analysis was performed using LS-DYNA. All parts analyzed are shells of thickness 6.350 mm, and are made of ASTM A36 Steel, which has the following properties.

- Modulus of Elasticity (E): $2.07 \cdot 10^5$ MPa
- Mass Density (ρ): $7.8 \cdot 10^3$ kg/m^3
- Poisson's Ratio (ν): 0.33

Analyses use the Reissner-Mindlin shell formulation. The bracket is taken with no boundary conditions (Figure 18), so has six rigid body displacement modes. Both of the other analyses assume boundary constraints as depicted in their accompanying figures (Figures 19 and 20).

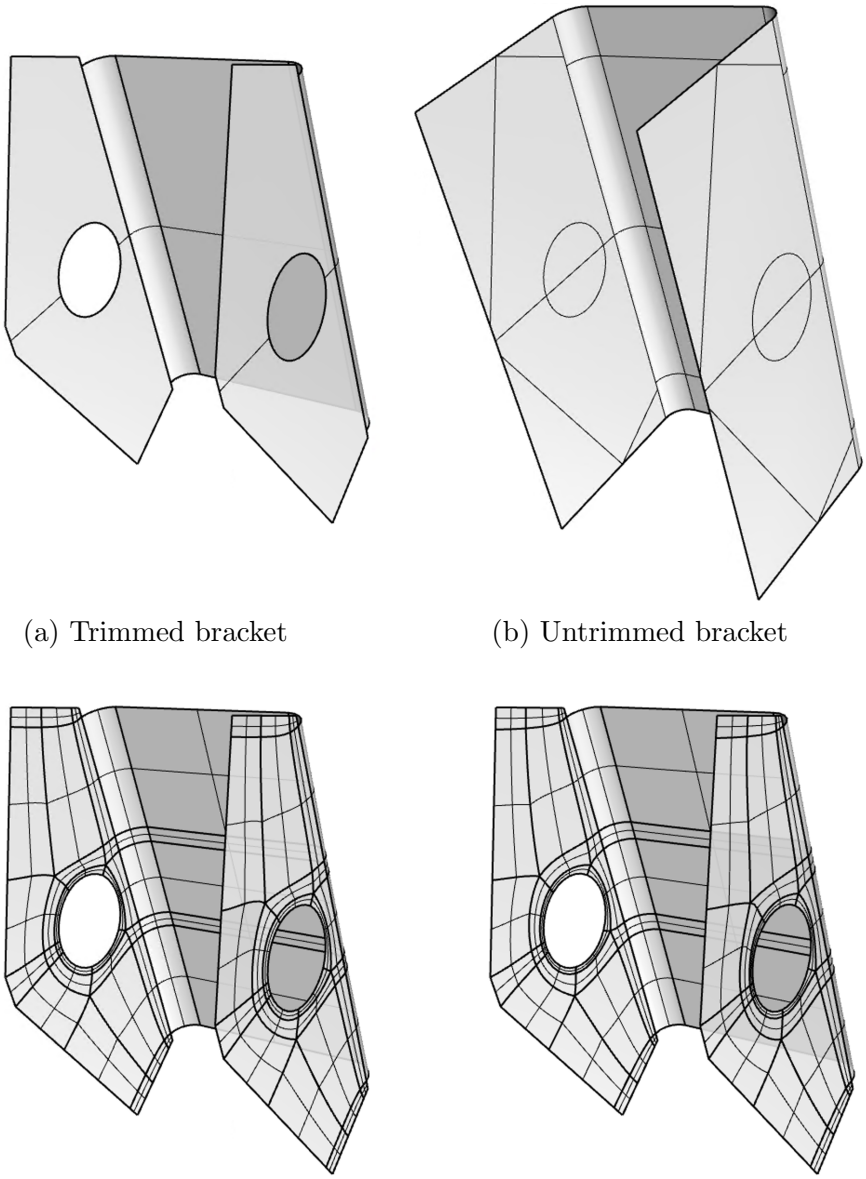

(a) Trimmed bracket

(b) Untrimmed bracket

(c) Reconstructed using [36]

(d) Reconstructed using present method

Figure 14: A bracket of the DEVCOM Generic Hull vehicle is converted into a trim-free watertight spline representation. Below, the reconstruction technique of [36] is compared against that of this method: all splines depicted are Bézier patches. Notice that while singularity locations for both are the same, the integral curves of this approach, being more conformal, are less straight than those of [36], which minimizes a Dirichlet-type energy.

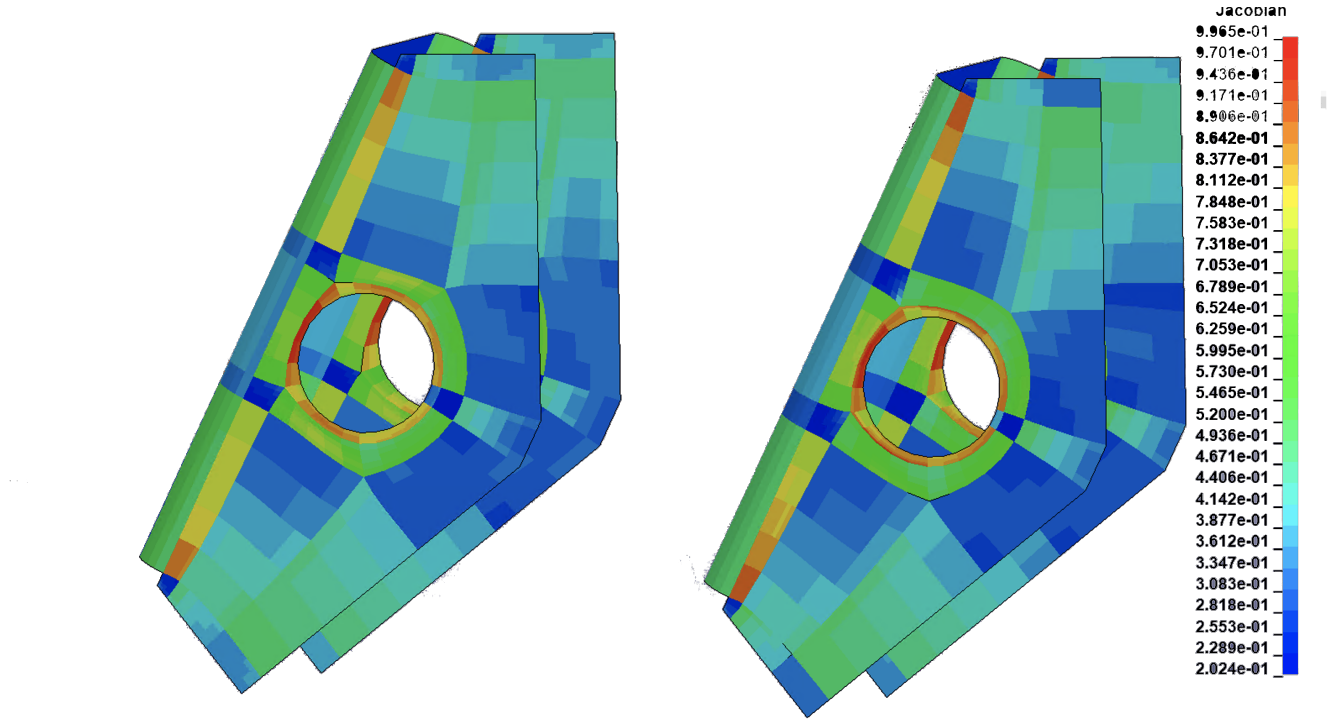

Figure 15: Jacobians within patches of the DEVCOM bracket rebuilt using the frame field method of [36] (left) and the proposed method of this work (right) are shown.

4.2. 1996 Dodge Neon

George Washington University's National Crash Analysis Center (NCAC) has performed a variety of finite element crash simulations for evaluation of safety of a number of commercial vehicles. One such model is the 1996 Dodge Neon [28], which was tested for frontal crash loading.

Though hundreds of parts comprise the actual vehicle, this work focuses on the evaluation of four: the vehicle firewall, the cabin's rear deck speaker support, the front-right shock house, and the outer-right shell member of the vehicle's chassis. These parts were selected due to their geometric and topological complexity. For each of these models, the original faceted model and the reconstructed watertight B-Rep are displayed side-by-side in Subfigures (a) and (b), respectively, of Figures 21, 22, 23, and 24.

When starting from a finite element mesh, geometric errors that are a by-product of feature removal, geometry clean-up, and other approximations typically made to facilitate finite element mesh generation are obviously inherited by the spline model. The sharp crease in Figure 21 and the sharp reentrant corners in the holes of Figure 24 are manifestations of this. Nevertheless, the spline models eliminate all triangles in FEM meshes, which are a liability in local nonlinear failure analysis, and thus are a significant improvement. However, many of these geometric errors can be fixed by smoothly mapping the spline model to the original CAD geometry. An L^2-best fitting would seem a simple and efficient procedure for this purpose. This is a topic for future research.

Isogeometric modal analyses are performed for refinements of each of the above-listed models. All analyses use the Reissner-Mindlin shell formulation. Material data for the NCAC finite element model, which was also used in these isogeometric analyses, was determined from coupon testing

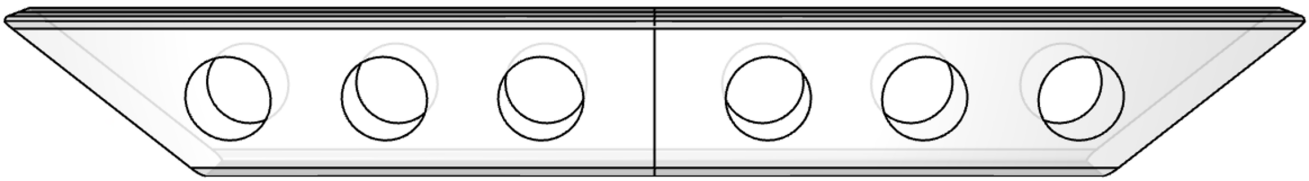

(a) Trimmed support beam

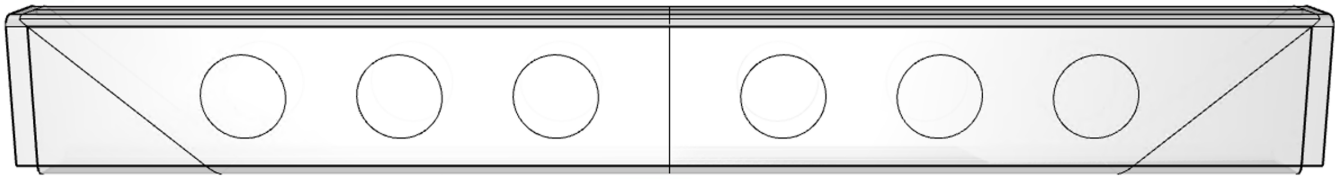

(b) Untrimmed support beam

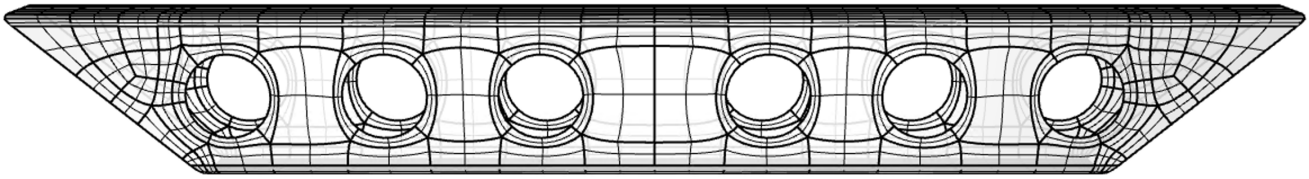

(c) Reconstructed support beam

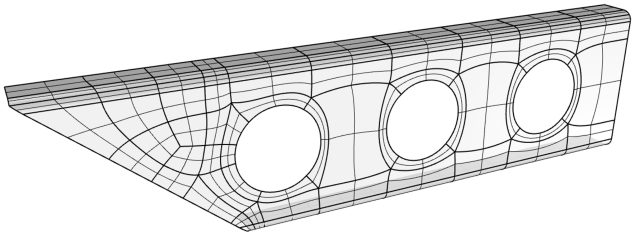

(d) Symmetric portion Bézier patches

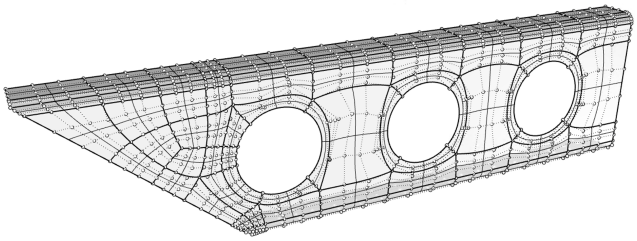

(e) Symmetric portion with control points and control mesh

Figure 16: A structural beam of the DEVCOM Generic Hull vehicle is converted into a trim-free watertight spline representation using bicubic Bézier patches.

[28]: the analyzed parts are all steel. All analyzed models have following mass density, modulus of elasticity, and Poisson's ratio:

- Modulus of Elasticity (E): $2.1 \cdot 10^5$ MPa
- Mass Density (ρ): $7.89 \cdot 10^3$ kg/m^3
- Poisson's Ratio (ν): 0.30

Thicknesses of shells are $0.735, 0.829, 0.96$, and 0.907 mm, respectively. Representative modes for the spline models are shown in the latter subfigures of Figures 21, 22, 23, and 24.

5. Conclusions

In this work, we presented a new framework to rebuild trimmed and faceted open midsurface geometries into isogeometric analysis-suitable spline spaces. First, we defined a generalized set of

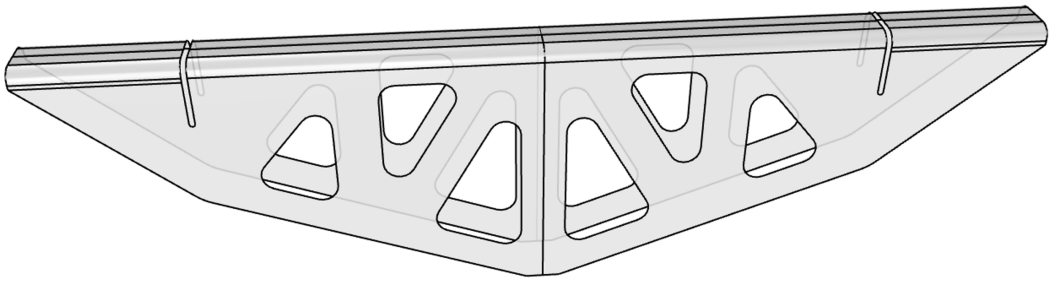

(a) Trimmed rounded support beam

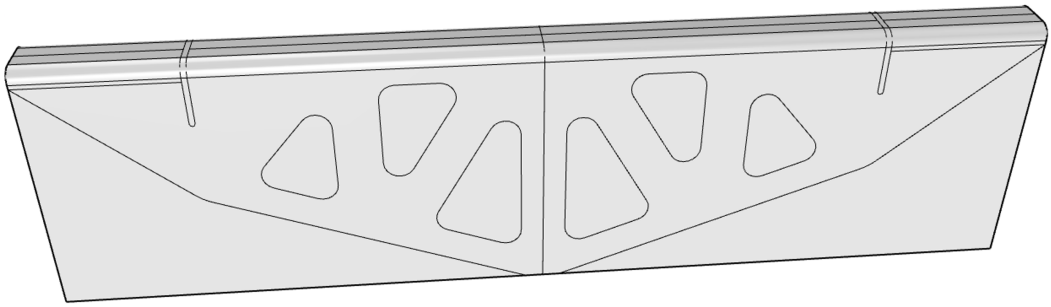

(b) Untrimmed rounded support beam

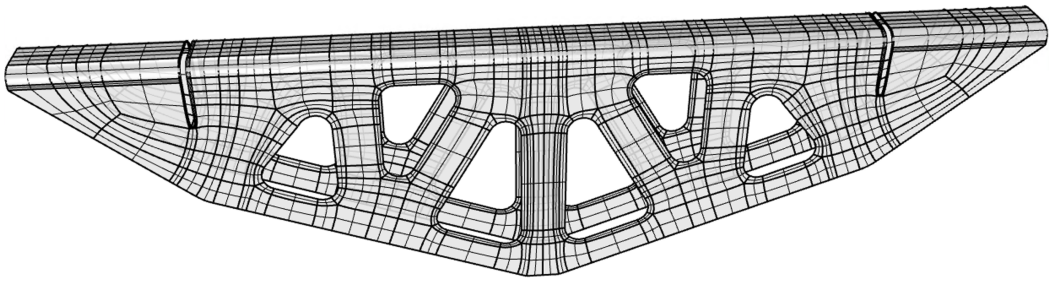

(c) Reconstructed rounded support beam

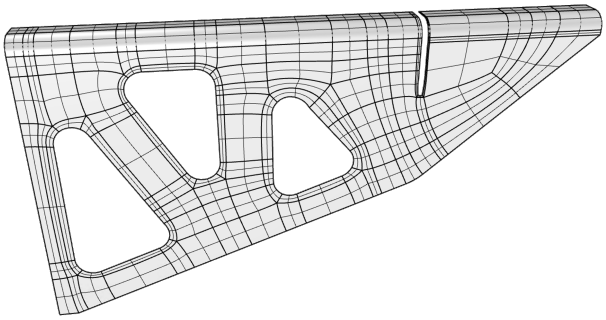

(d) Symmetric portion Bézier patches

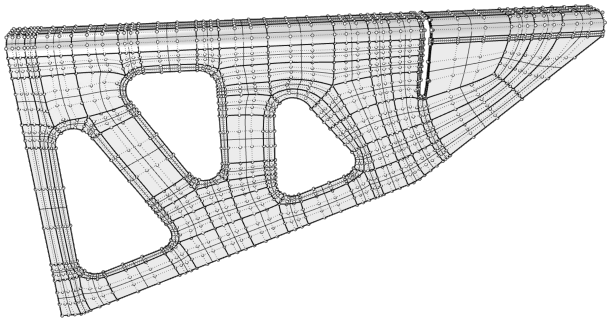

(e) Symmetric portion with control points and control mesh

Figure 17: A rounded structural support beam of the DEVCOM Generic Hull vehicle is converted into a trim-free watertight spline representation using bicubic Bézier patches.

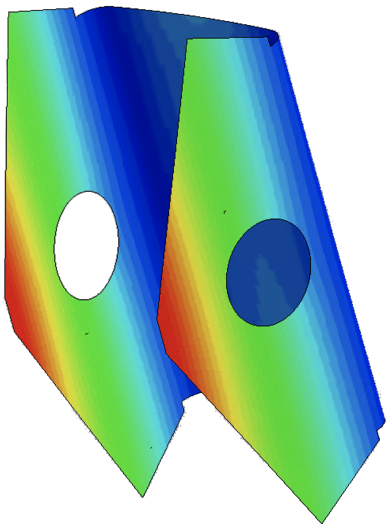

(a) Mode 7: 194 Hz

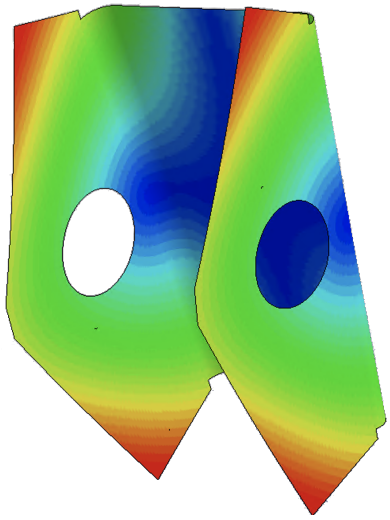

(b) Mode 8: 196 Hz

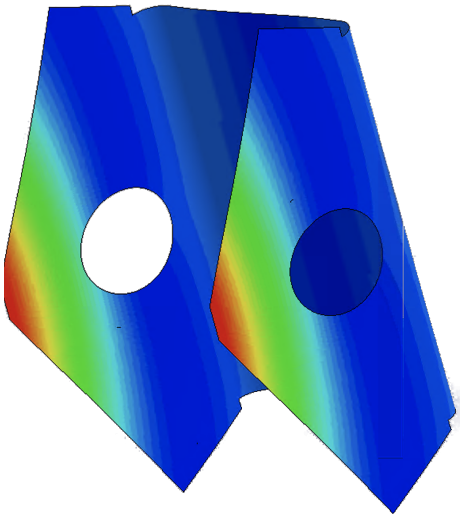

(c) Mode 9: 401 Hz

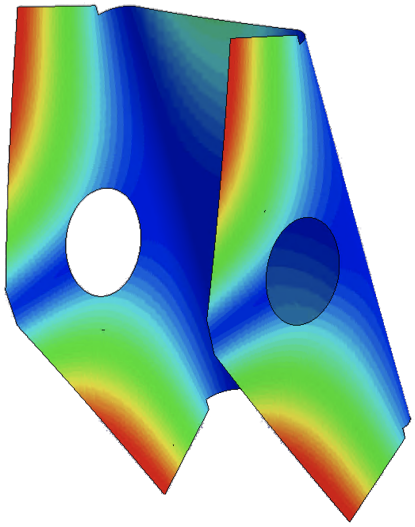

(d) Mode 10: 412 Hz

Figure 18: Isogeometric modal analyses of the reparameterized bracket of Figure 14 (d) with each Bézier patch uniformly subdivided to have 8×8 patches by insertion of knots with single multiplicity.

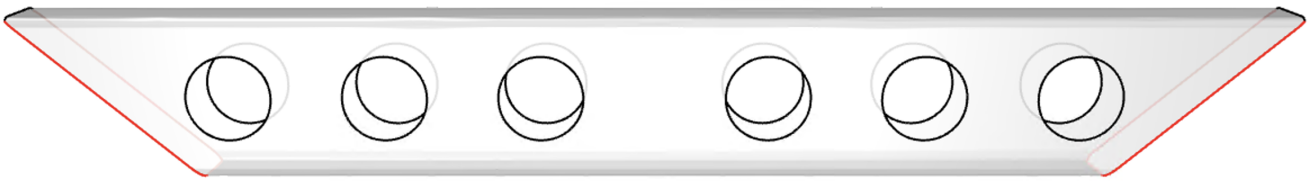

(a) Beam with fixed displacements on red portion of boundary

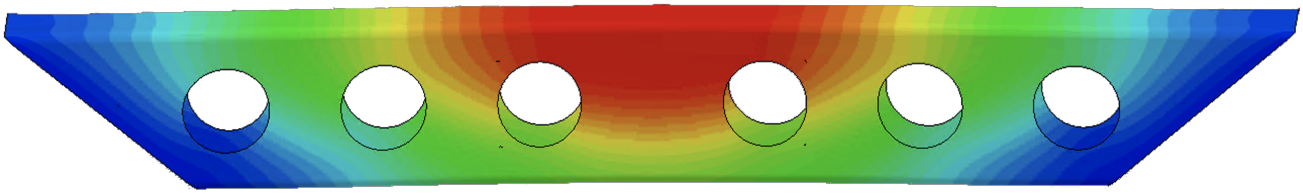

(b) Mode 1: 443 Hz

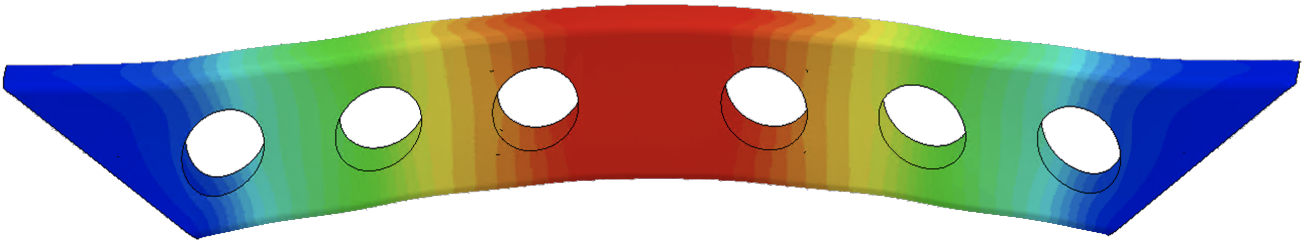

(c) Mode 2: 753 Hz

Figure 19: Isogeometric modal analysis of the reparameterized structural beam of Figure 16 with pinned supports (zero displacements) on the red portion of the boundary. The Bézier patches of Figure 16 were uniformly subdivided into 8×8 patches by insertion of knots with single multiplicity.

criteria for a surface triangulation that, if satisfied, generate a quadrilateral layout. Based on this theory, we combined the tools of discrete surface Ricci flow [42, 90] with a constrained minimization against an inversion-precluding energy [52, 65, 84, 85] with layout-inducing penalty constraints. The methodology assures that the computed parameterizations are locally injective, a necessary criterion frequently not satisfied by many current quadrilateral parameterization techniques [7, 8, 24, 36, 54]. The defined framework was used to rebuild topologically and geometrically complicated members of both the US Army's DEVCOM Generic Hull vehicle [23] and the National Crash Analysis Center's 1996 Dodge Neon finite element model [28], including models for which current state-of-the-art techniques fail [35, Appendix B]. We show the viability of each of the rebuilt models by using them for isogeometric modal analyses using the commercial solver LS-DYNA.

While the proposed framework offers a feature-aware technique to generate spline surfaces suitable for isogeometric analysis, additional work remains. First, the proposed methodology focuses on reconstruction of open surfaces. While there is no theoretical reason that the technique cannot extend to closed surfaces other than potential holonomy issues for unusual and pathological singularity configurations [15, 50], the methodology has not yet been explored on these surfaces. Closed surfaces pose an additional challenge, as well, because they will not typically satisfy Property **Q5** of Definition 2.1, as will most open surfaces.

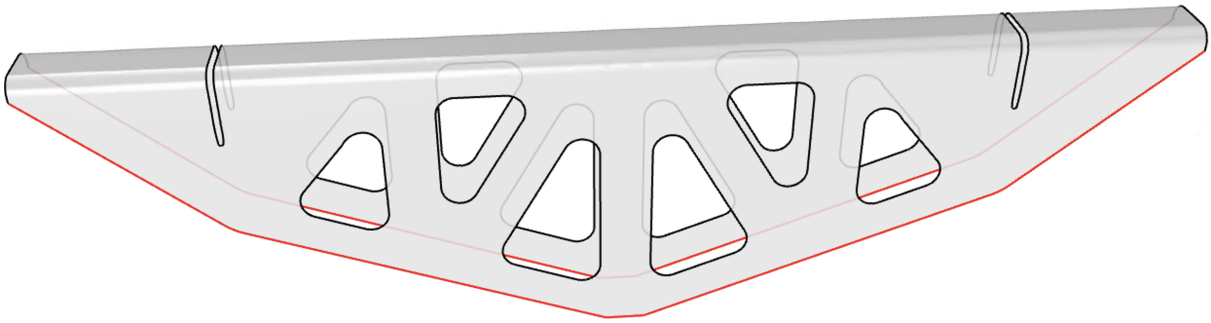

(a) Beam with fixed displacements on red portion of boundary

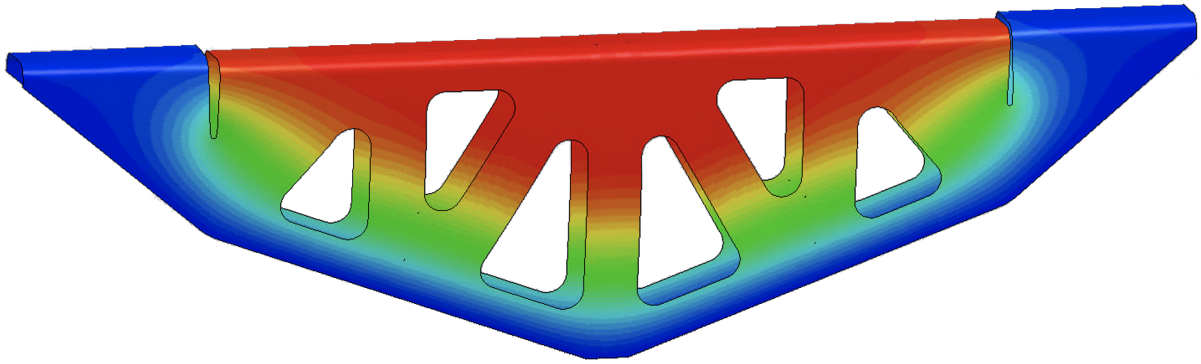

(b) Mode 1: 132 Hz

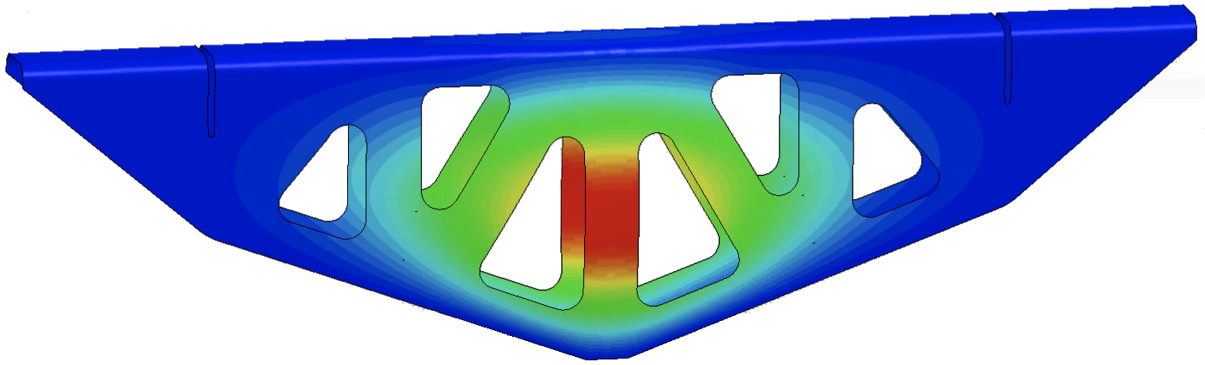

(c) Mode 2: 323 Hz

Figure 20: Isogeometric modal analysis of the reparameterized structural beam of Figure 17 with pinned supports (zero displacements) on the red portion of the boundary. The Bézier patches of Figure 17 were uniformly subdivided into 8×8 patches by insertion of knots with single multiplicity.

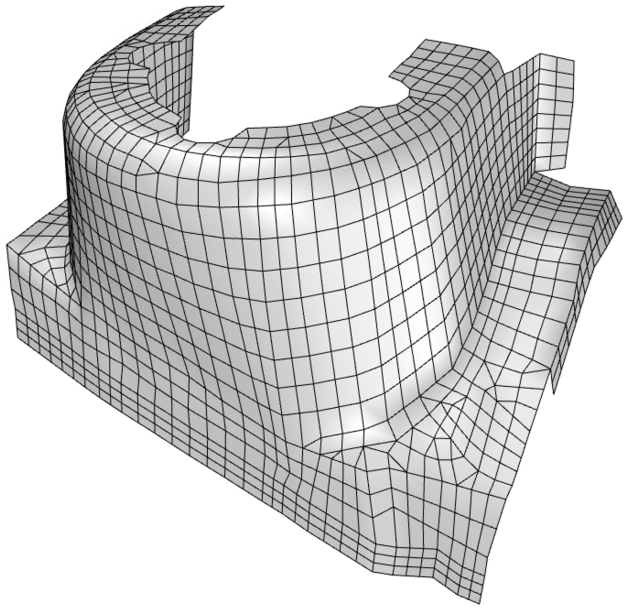

(a) Mixed FEM mesh

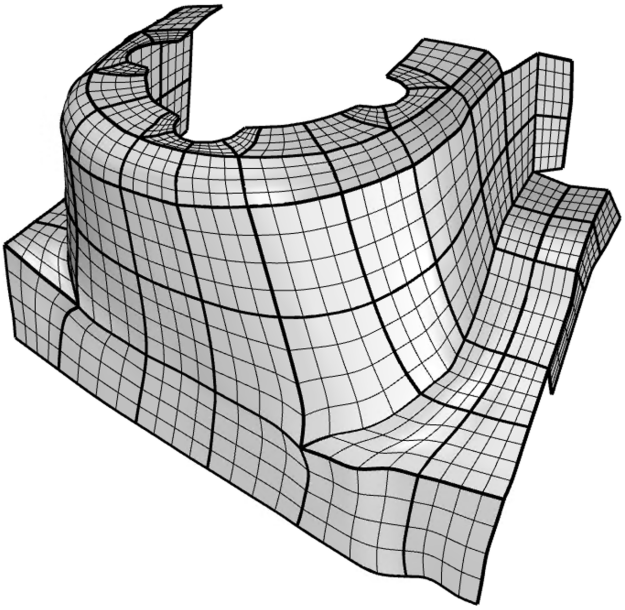

(b) Spline reconstruction

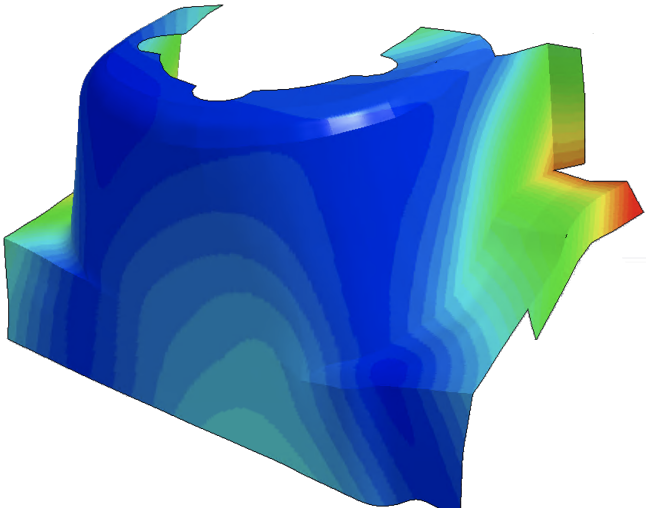

(c) Mode 7: 32.2 Hz

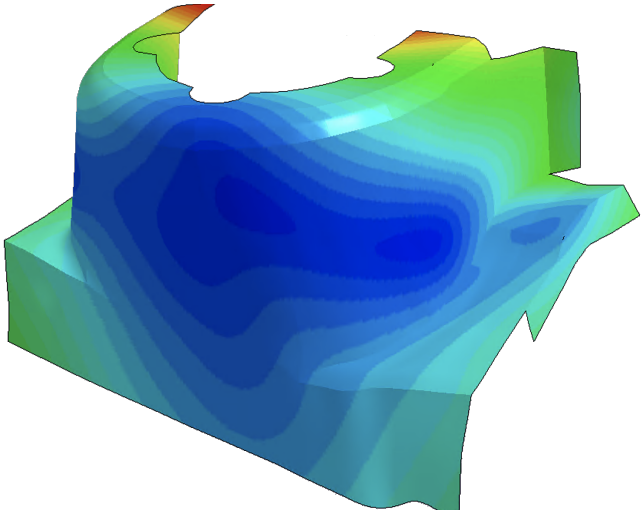

(d) Mode 8: 34.4 Hz

Figure 21: The front right shock house from a finite element mesh of a 1996 Dodge Neon [28] is rebuilt as a set of bicubic NURBS patches, each with 7×7 control points (i.e. 4×4 Bézier patches), with at least C^2 continuity on the interior of each patch and C^0 continuity between patches. After uniform refinement to 8×8 Bézier patches for each patch, modal analysis is performed on the model with free boundaries.

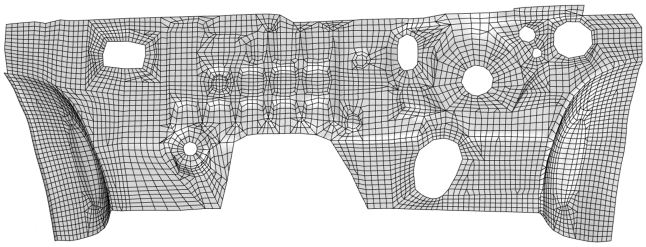

(a) Mixed FEM mesh

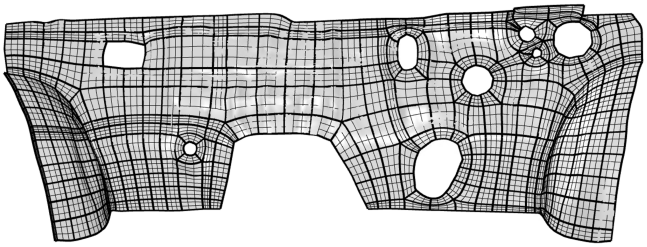

(b) Spline reconstruction

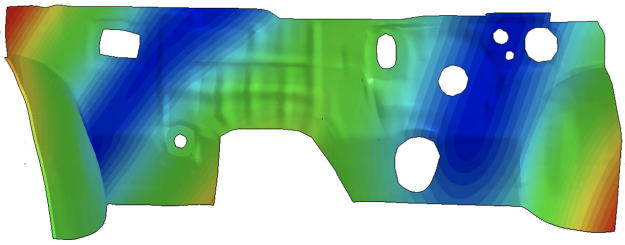

(c) Mode 7: 5.4 Hz

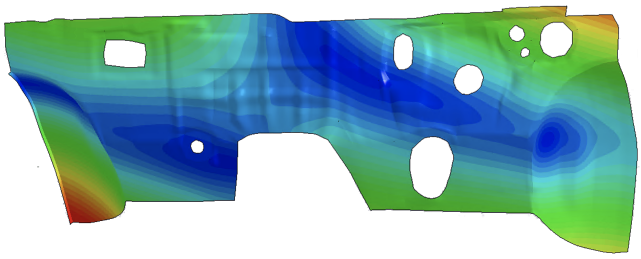

(d) Mode 8: 5.7 Hz

Figure 22: The cabin firewall from a finite element mesh of a 1996 Dodge Neon [28] is rebuilt as a set of bicubic NURBS patches, each with 6×6 control points (i.e. 3×3 Bézier patches), with at least C^2 continuity on the interior of each patch and C^0 continuity between patches. After uniform refinement to 12×12 Bézier patches for each patch, modal analysis is performed on the model with free boundaries.

Next, the parameterization framework needs alternative ways to select singularities. The current framework relies on a Dirichlet-type energy with guarantees for valid singularity positions only if the input geometry is sufficiently smooth [47]: these smoothness conditions may not hold on highly-featured structural and mechanical surfaces. Furthermore, automatic placement of singularities is limited to valence three and five singularities [47], though many geometries of interest may benefit from higher-valence cones.

Finally, additional research should focus on more advanced spline fitting techniques. The current technique employs linear interpolation between integral curves defining the boundary of a patch in the quadrilateral layout. For more nonlinear parameterizations or geometries with significant curvature in their domains, this technique will be insufficient to capture these nonlinear features and would require additional layout subdivision at the expense of more degrees of freedom and reduced continuity. Instead, manifold splines such as unstructured T-splines [16, 78, 89] or U-splines [86] may be necessary. Additional research will also need to focus on how to fit splines produced on the triangulation back to the original trimmed CAD domain. Because geometries used herein are predominantly flat, reconstruction from the triangulation to the original geometry was fairly straightforward. An ultimate objective is minimizing the need for user intervention in the process.

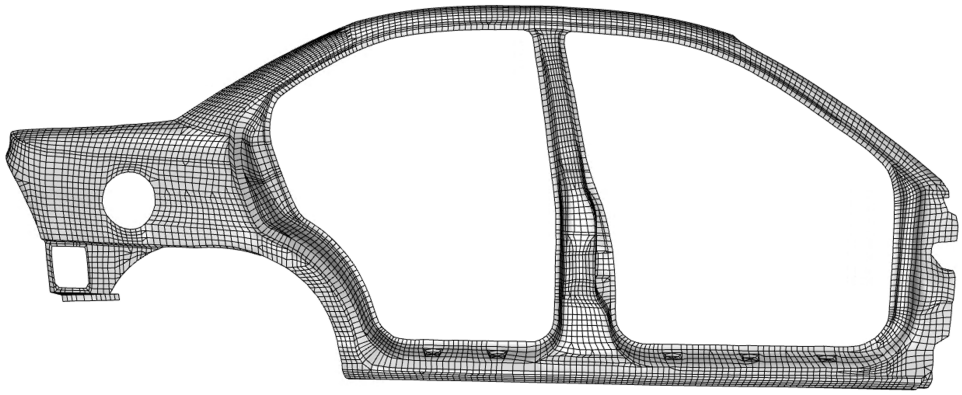

(a) Mixed FEM mesh

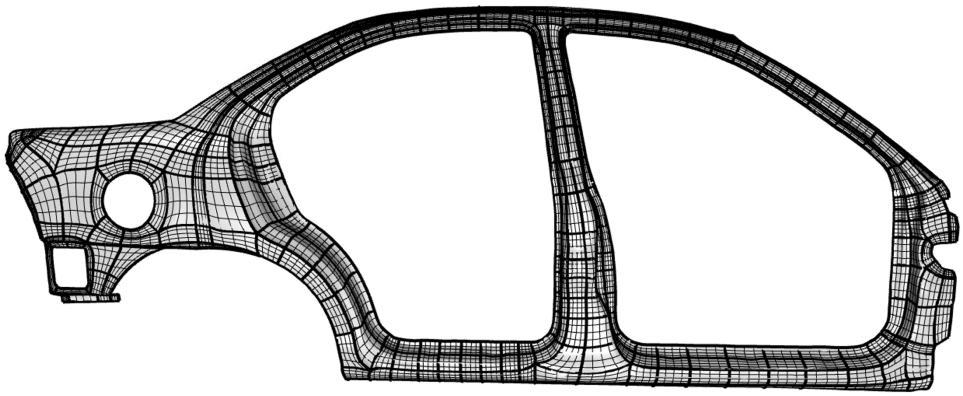

(b) Spline reconstruction

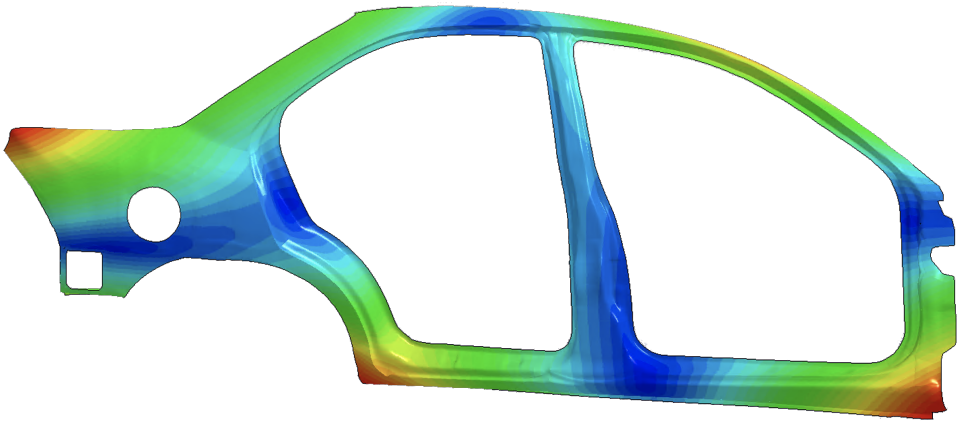

(c) Mode 7: 3.4 Hz

Figure 23: The right outer shell of the cabin chassis from a finite element mesh of a 1996 Dodge Neon [28] is rebuilt as a set of bicubic NURBS patches, each with 7×7 control points (i.e. 4×4 Bézier patches), with at least C^2 continuity on the interior of each patch and C^0 continuity between patches. After uniform refinement to 8×8 Bézier patches for each patch, modal analysis is performed on the model with free boundaries.

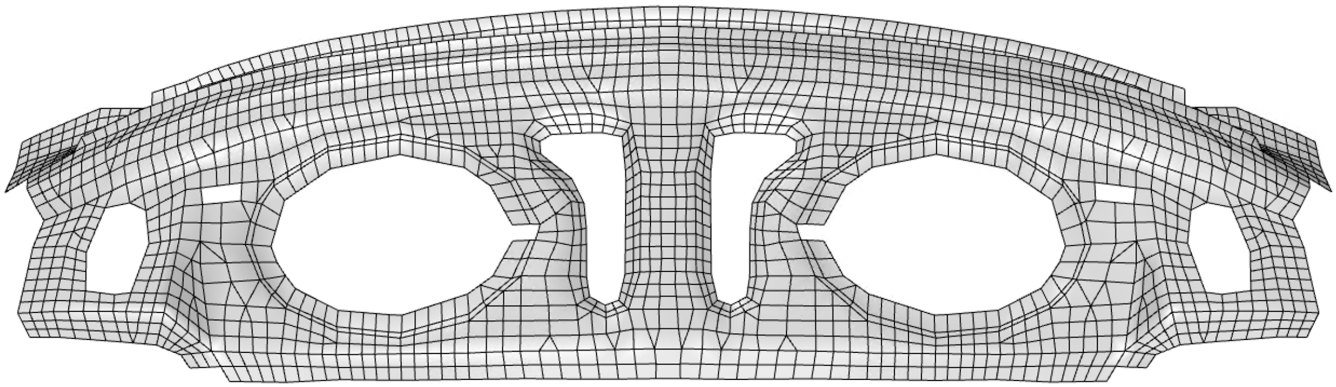

(a) Mixed FEM mesh

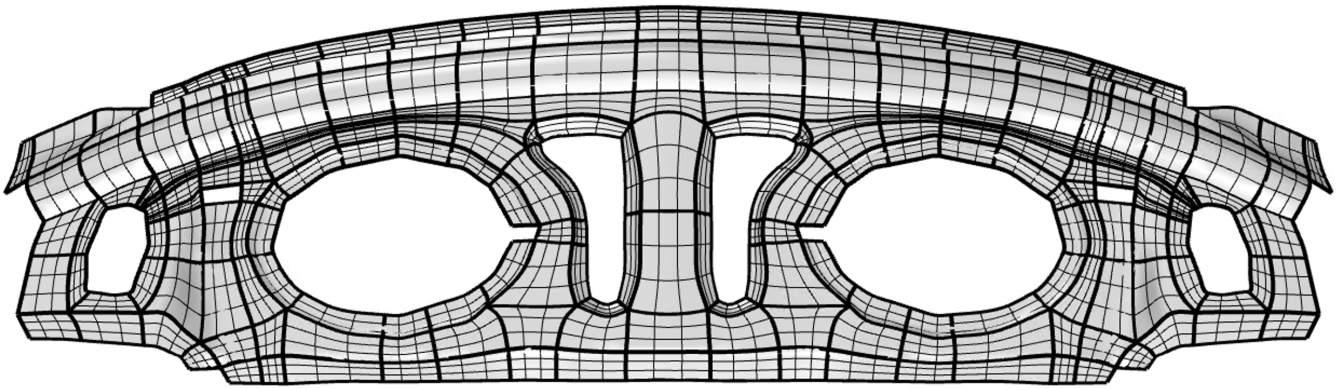

(b) Spline reconstruction

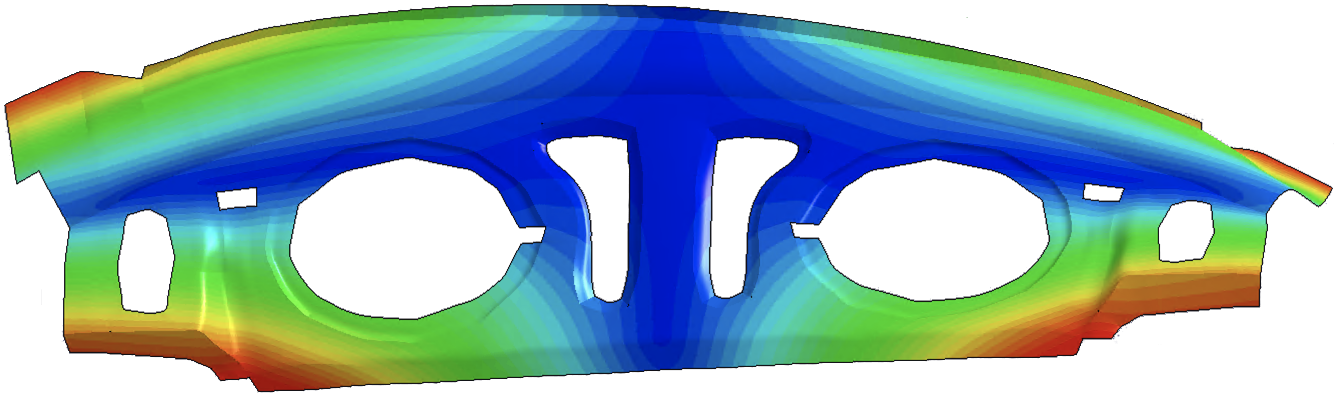

(c) Mode 7: 17.6 Hz

Figure 24: The frame supporting the rear speakers of the cabin from a finite element mesh of a 1996 Dodge Neon [28] is rebuilt as a set of bicubic NURBS patches, each with 6×6 control points (i.e. 3×3 Bézier patches), with at least C^2 continuity on the interior of each patch and C^0 continuity between patches. After uniform refinement to 12×12 Bézier patches for each patch, modal analysis is performed on the model with free boundaries.

Acknowledgements

The authors would like to thank Attila Nagy and the team at LS-DYNA for their assistance performing isogeometric modal analyses.

Thomas J. R. Hughes and Kendrick Shepherd were partially supported by United States Department of Defense Navy Contract N6833518C0014 through a subcontract with Coreform, LLC, which is gratefully acknowledged.

References

[1] H. Al Akhras, T. Elguedj, A. Gravouil, and M. Rochette. Towards an automatic isogeometric analysis suitable trivariate models generation—application to geometric parametric analysis. *Comput. Methods Appl. Mech. Engrg.*, 316:623–645, 2017. https://doi.org/10.1016/j.cma.2016.09.030.

[2] I. Babuška and M. Suri. Locking effects in the finite element approximation of elasticity problem. *Numer. Math.*, 62:439–463, 1992. https://doi.org/10.1007/BF01396238.

[3] L. Beirão da Veiga, T. J. R. Hughes, J. Kiendl, C. Lovadina, J. Niiranen, A. Reali, and H. Speleers. A locking-free model for Reissner-Mindlin plates: Analysis and isogeometric implementation via NURBS and triangular NURPS. *Math. Models Methods in Appl. Sci.*, 25(8):1519–1551, 2015. https://doi.org/10.1142/S0218202515500402.

[4] T. Belytschko, W. K. Liu, B. Moran, and K. Elkhodary. *Nonlinear Finite Elements for Continua and Structures*. John Wiley & Sons, Inc., New York, 2 edition, 2014.

[5] S. E. Benzley, E. Perry, K. Merkley, B. Clark, and G. Sjaardema. A comparison of all hexagonal and all tetrahedral finite element meshes for elastic and elastic-plastic analysis. In *Proc. 4th International Meshing Roundtable*, pages 179–192, Albuquerque, NM, 1995. Sandia National Laboratories.

[6] P. T. Boggs, A. Althsuler, A. R. Larzelere, E. J. Walsh, R. L. Clay, and M. F. Hardwick. DART system analysis. Report, Sandia National Laboratories, August 2005, https://doi.org/10.2172/876325.

[7] D. Bommes, M. Campen, H.-C. Ebke, P. Alliez, and L. Kobbelt. Integer-grid maps for reliable quad meshing. *ACM Transactions on Graphics*, 32(4), 2013. https://doi.org/10.1145/2461912.2462014.

[8] D. Bommes, H. Zimmer, and L. Kobbelt. Mixed-integer quadrangulation. In *ACM SIGGRAPH 2009 Papers*, SIGGRAPH '09, Article No. 77. ACM, 2009, https://doi.org/10.1145/1576246.1531383.

[9] M. Breitenberger. *CAD-integrated Design and analysis of shell structures*. PhD thesis, Technical University of Munich, Germany, 2016, http://mediatum.ub.tum.de/?id=1311417.

[10] M. Breitenberger, A. Apostolatos, B. Philipp, R. Wüchner, and K. U. Bletzinger. Analysis in computer aided design: Nonlinear isogeometric B-Rep analysis of shell structures. *Comput. Methods Appl. Mech. Engrg.*, 284:401–457, 2015. https://doi.org/10.1016/j.cma.2014.09.033.

[11] S. B. Brunnermeier and S. A. Martin. Interoperability cost analysis of the us automotive supply chain. *Supply Chain Manag.*, 7(2):71–82, May 2002. https://doi.org/10.1108/13598540210425821.

[12] G. Brunnett. Geometric design with trimmed surfaces. In H. Hagen, G. Farin, and H. Noltemeier, editors, *Geometric Modelling*, volume 10 of *Computing Supplement*, pages 101–115. Springer, 1989, https://doi.org/10.1007/978-3-7091-7584-2_7.

[13] M. Campen, D. Bommes, and L. Kobbelt. Dual loops meshing: Quality quad layouts on manifolds. *ACM Trans. Graph.*, 31(4):Article No. 110, 2012. https://doi.org/10.1145/2185520.2185606.

[14] M. Campen, D. Bommes, and L. Kobbelt. Quantized global parameterization. *ACM Trans. Graph.*, 34(6):Article No. 192, November 2015. https://doi.org/10.1145/2816795.2818140.

[15] M. Campen, H. Shen, J. Zhou, and D. Zorin. Seamless parametrization with arbitrary cones for arbitrary genus. *ACM Trans. Graph.*, 39(1):Article No. 2, December 2019. https://doi.org/10.1145/3360511.

[16] H. Casquero, X. Wei, D. Toshniwal, A. Li, T. J. R. Hughes, J. Kiendl, and Y. J. Zhang. Seamless integration of design and Kirchhoff-Love shell analysis using analysis-suitable unstructured T-splines. *Comput. Methods Appl. Mech. Engrg.*, 360:Article No. 112765, 2020. https://doi.org/10.1016/j.cma.2019.112765.

[17] W. Chen, X. Zheng, J. Ke, N. Lei, Z. Luo, and X. Gu. Quadrilateral mesh generation I: Metric based method. *Comput. Methods Appl. Mech. Engrg.*, 356:652–668, 2019. https://doi.org/10.1016/j.cma.2019.07.023.

[18] B. Chow and F. Luo. Combinatorial Ricci flows on surfaces. *J. Differential Geom.*, 63(1):97–129, 2003. https://doi.org/10.4310/jdg/1080835659.

[19] F. de Prenter, C. V. Verhoosel, and E. H. van Brummelen. Preconditioning immersed isogeometric finite element methods with application to flow problems. *Comput. Methods Appl. Mech. Eng.*, 348:604–631, 2019. https://doi.org/10.1016/j.cma.2019.01.030.

[20] F. de Prenter, C. V. Verhoosel, G. J. van Zwieten, and E. H. van Brummelen. Condition number analysis and preconditioning of the finite cell method. *Comput. Methods Appl. Mech. Eng.*, 316:297–327, 2017. https://doi.org/10.1016/j.cma.2016.07.006.

[21] O. Diamanti, A. Vaxman, D. Panozzo, and O. Sorkine-Hornung. Integrable PolyVector fields. *ACM Trans. Graph.*, 34(4):Article No. 38, July 2015. https://doi.org/10.1145/2766906.

[22] S. Dong, P.-T. Bremer, M. Garland, V. Pascucci, and J. Hart. Spectral surface quadrangulation. *ACM Trans. Graph.*, 25(3):1057–1066, 2006. https://doi.org/10.1145/1141911.1141993.

[23] D. Dooge, R. Dwarampudi, G. Schaffner, A. Miller, R. Thyagarajan, V. Madanmohan, and V. Babu. Evolution of occupant survivability simulation framework using FEM-SPH coupling. *2011 NDIA Ground Vehicle Systems Engineering and Technology Symposium (GVSETS), Dearborn, MI, Aug 9–11*, 2011. DTIC Report #ADA547566, TARDEC Registration #22044.

[24] H.-C. Ebke, D. Bommes, M. Campen, and L. Kobbelt. QEx: Robust quad mesh extraction. *ACM Trans. Graph.*, 32(6):Article No. 168, 2013. https://doi.org/10.1145/2508363.2508372.

[25] J. A. Evans, Y. Bazilevs, I. Babuška, and T. J. R. Hughes. n-widths, sup-infs, and optimality ratios for the k-version of the isogeometic finite element method. *Comput. Methods Appl. Mech. Engrg.*, 198(21–26):1726–1741, 2009. https://doi.org/10.1016/j.cma.2009.01.021.

[26] G. Farin. *Curves and Surfaces for CAGD: A Practical Guide*. Morgan Kaufmann Publishers, San Francisco, CA, 5 edition, 2002, https://doi.org/10.1016/B978-1-55860-737-8.X5000-5.

[27] R. T. Farouki. Closing the gap between CAD model and downstream application. *SIAM News*, 32(5):1–3, 1999. https://archive.siam.org/news/news.php?id=743.

[28] George Washington University. Finite element model of dodge neon. Technical report, George Washington University, Virginia Campus, 2006, http://web.archive.org/web/20160408180243/http://www.ncac.gwu.edu/vml/models.html.

[29] X. Gu, R. Guo, F. Luo, J. Sun, and T. Wu. A discrete uniformization theorem for polyhedral surfaces II. *J. Differ. Geom.*, 109(3):431–466, 2018. https://doi.org/10.4310/jdg/1531188190.

[30] X. Gu and S.-T. Yau. Global conformal surface parameterization. In L. Kobbelt, P. Schröeder, and H. Hoppe, editors, *Eurographics Symposium on Geometry Processing*, pages 127–137. The Eurographics Association, 2003, https://doi.org/10.2312/SGP/SGP03/127-137.

[31] X. D. Gu, F. Lou, J. Sun, and T. Wu. A discrete uniformization theorem for polyhedral surfaces. *J. Differ. Geom.*, 109(2):223–256, 2018. https://doi.org/10.4310/jdg/1527040872.

[32] X. D. Gu and S.-T. Yau. Computational conformal geometry. In S.-T. Yau, K. Liu, and L. Ji, editors, *Advanced Lectures in Mathematics (ALM)*, volume 3. International Press, Somerville, MA, U.S.A., 2008.

[33] Y. Guo, H. Do, and M. Ruess. Isogeometric stability analysis of thin shells: from simple geometries to engineering models. *Int. J. Numer. Methods. Eng.*, 118(8):433–458, 2019. https://doi.org/10.1002/nme.6020.

[34] Y. Guo, J. Heller, T. J. R. Hughes, M. Ruess, and D. Schillinger. Variationally consistent isogeometric analysis of trimmed thin shells at finite deformations, based on the STEP exchange format. *Comput. Methods Appl. Mech. Engrg.*, 336:39–79, 2018. https://doi.org/10.1016/j.cma.2018.02.027.

[35] R. R. Hiemstra. *Enabling Higher Order Isogeometric Analysis for Applications in Structural Mechanics*. PhD thesis, The University of Texas at Austin, Austin, TX, 2019, https://doi.org/10.26153/tsw/5857.

[36] R. R. Hiemstra, K. M. Shepherd, M. J. Johnson, L. Quan, and T. J. R. Hughes. Towards untrimmed NURBS: CAD embedded reparameterization of trimmed B-rep geometry using frame-field guided global parameterization. *Comput. Methods in Appl. Mech. Engrg.*, 369:Article No. 113227, September 2020. https://doi.org/10.1016/j.cma.2020.113227.

[37] K. Hu and Y. J. Zhang. Centroidal Voroni tessellation based polycube construction for adaptive all-hexahedral mesh generation. *Comput. Methods Appl. Mech. Engrg.*, 305:405–421, 2016. https://doi.org/10.1016/j.cma.2016.03.021.

[38] J. F. P. Hudson. *Piecewise Linear Topology*. W. A. Benjamin, Inc., New York, NY, 1969.

[39] T. J. R. Hughes, J. A. Cottrell, and Y. Bazilevs. Isogeometric analysis: CAD, finite elements, NURBS, exact geometry and mesh refinement. *Comput. Methods Appl. Mech. Engrg.*, 194(39-41):4135–4195, 2005. https://doi.org/10.1016/j.cma.2004.10.008.

[40] T. J. R. Hughes, A. Reali, and G. Sangalli. Duality and unified analysis of discrete approximations in structural dynamics and wave propagation: Comparison of p-method finite elements with k-method NURBS. *Comput. Methods Appl. Mech. Engrg.*, 197(49-50):4104–4124, 2008.

[41] T. J. R. Hughes, A. Reali, and G. Sangalli. Efficient quadrature for NURBS-based isogeometric analysis. *Comput. Methods Appl. Mech. Engrg.*, 199(5-8):301–313, 2010. https://doi.org/10.1016/j.cma.2008.12.004.

[42] M. Jin, J. Kim, F. Luo, and X. Gu. Discrete surface Ricci flow. *IEEE Trans. Vis. Comput. Graph.*, 14(5):1030–1043, September 2008. https://doi.org/10.1109/TVCG.2008.57.

[43] F. Kälberer, M. Nieser, and K. Polthier. QuadCover - surface parameterization using branched coverings. *Computer Graphics Forum*, 26(3):375–384, 2007. https://doi.org/10.1111/j.1467-8659.2007.01060.x.

[44] S. Katz and T. W. Sederberg. Genus of the intersection curve of two rational surface patches. *Comput. Aided Geom. Design*, 5(3):253–258, 1988. https://doi.org/10.1016/0167-8396(88)90006-4.

[45] J. Kiendl, K.-U. Bletzinger, J. Linhard, and R. Wuchner. Isogeometric shell analysis with Kirchhoff–Love elements. *Comput. Methods Appl. Mech. Engrg.*, 198(49–52):3902–3914, 2009. https://doi.org/10.1016/j.cma.2009.08.013.

[46] H.-J. Kim, Y.-D. Seo, and S.-K. Youn. Isogeometric analysis for trimmed CAD surfaces. *Comput. Methods Appl. Mech. Engrg.*, 198(37–40):2982–2995, 2009. https://doi.org/10.1016/j.cma.2009.05.004.

[47] F. Knöppel, K. Crane, U. Pinkall, and P. Schröder. Globally optimal direction fields. *ACM Trans. Graph.*, 32(4):Article No. 59, 2013. https://doi.org/10.1145/2461912.2462005.

[48] N. Lei, X. Zheng, J. Jiang, Y.-Y. Lin, and D. X. Gu. Quadrilateral and hexahedral mesh generation based on surface foliation theory. *Comput. Methods Appl. Mech. Engrg.*, 316:758–781, 2017. https://doi.org/10.1016/j.cma.2016.09.044.

[49] N. Lei, X. Zheng, Z. Luo, and D. X. Gu. Quadrilateral and hexahedral mesh generation based on surface foliation theory II. *Comput. Methods Appl. Mech. Engrg.*, 321:406–426, 2017. https://doi.org/10.1016/j.cma.2017.04.012.

[50] N. Lei, X. Zheng, Z. Luo, F. Luo, and X. Gu. Quadrilateral mesh generation II: Meromorphic quartic differentials and Abel-Jacobi condition. *Comput. Methods Appl. Mech. Engrg.*, 366:Article No. 112980, 2020. https://doi.org/10.1016/j.cma.2020.112980.

[51] L. Leidinger, M. Breitenberger, A. M. Bauer, S. Hartmann, R. Wüchner, K.-U. Bletzinger, F. Duddeck, and L. Song. Explicit dynamic isogeometric B-Rep analysis of penalty-coupled trimmed NURBS shells. *Comput. Methods Appl. Mech. Engrg.*, 351:891–927, 2019. https://doi.org/10.1016/j.cma.2019.04.016.

[52] L. Liu, C. Ye, R. Ni, and X.-M. Fu. Progressive parameterizations. *ACM Trans. Graph.*, 37(4):Article No. 41, August 2018. https://doi.org/10.1145/3197517.3201331.

[53] X. Luo, M. Shephard, and J.-F. Remacle. Influence of geometric approximation on the accuracy of higher order methods. Technical report, Scientific Computation Research Center, Rensselaer Polytechnic Institute, Troy, NY, 2001.

[54] M. Lyon, M. Campen, and L. Kobbelt. Quad layouts via constrained T-mesh quantization. *Comput. Graph. Forum*, 40(2), 2021.

[55] T. Maquart, Y. Wenfeng, T. Elguedj, A. Gravouil, and M. Rochette. 3D volumetric isotopological meshing for finite element and isogeometric based reduced order modeling. *Comput. Methods Appl. Mech. Engrg.*, 362:Article No. 112809, 2020. https://doi.org/10.1016/j.cma.2019.112809.

[56] M. Marinov, M. Amagliani, and P. Charrot. Boundary conforming mesh to T-NURCC surface conversion. *Comput. Graph.*, 82:94–105, 2019. https://doi.org/10.1016/j.cag.2019.05.012.

[57] B. Marussig, R. Hiemstra, and T. J. R. Hughes. Improved conditioning of isogeometric analysis matrices for trimmed geometries. *Comput. Methods Appl. Mech. Eng.*, 334:79–110, 2018. https://doi.org/10.1016/j.cma.2018.01.052.

[58] B. Marussig and T. J. R. Hughes. A review of trimming in isogeometric analysis: Challenges, data exchange and simulation aspects. *Arch. Comput. Methods Eng.*, 25:1–69, 2017. https://doi.org/10.1007/s11831-017-9220-9.

[59] B. Marussig, J. Zechner, G. Beer, and T.-P. Fries. Stable isogeometric analysis of trimmed geometries. *Comput. Methods Appl. Mech. Engrg.*, 316:497–521, 2017. https://doi.org/10.1016/j.cma.2016.07.040.

[60] A. P. Nagy and D. J. Benson. On the numerical integration of trimmed isogeometric elements. *Comput. Methods Appl. Mech. Eng.*, 284:165–185, 2015. https://doi.org/10.1016/j.cma.2014.08.002.

[61] N. Nguyen-Thanh, N. Valizadeh, M. N. Nguyen, H. Nguyen-Xuan, X. Zhuang, P. Areias, G. Zi, Y. Bazilevs, L. de Lorenzis, and T. Rabczuk. An extended isogeometric thin shell analysis based on Kirchhoff-Love theory. *Comput. Methods Appl. Mech. Eng.*, 284:265–291, 2015. https://doi.org/10.1016/j.cma.2014.08.025.

[62] B. Oesterle, E. Ramm, and M. Bischoff. A shear deformable, rotation-free isogeometric shell formulation. *Comput. Methods Appl. Mech. Engrg.*, 307:235–255, 2016. https://doi.org/10.1016/j.cma.2016.04.015.

[63] D. Panozzo, E. Puppo, M. Tarini, and O. Sorkine-Hornung. Frame fields: Anisotropic and non-orthogonal cross fields. *ACM Trans. Graph.*, 33(4):Article No. 134, 2014. https://doi.org/10.1145/2601097.2601179.

[64] V. Puzyrev, Q. Deng, and V Calo. Spectral approximation properties of isogeometric analysis with variable continuity. *Comput. Methods Appl. Mech. Eng.*, 334:22–39, 2018. https://doi.org/10.1016/j.cma.2018.01.042.

[65] M. Rabinovich, R. Poranne, D. Panozzo, and O. Sorkine-Hornung. Scalable locally injective mappings. *ACM Trans. Graph.*, 36:Article No. 16, April 2017. https://doi.org/10.1145/2983621.

[66] M. Randrianarivony. *Geometric processing of CAD data and meshes as input of integral equation solvers*. PhD thesis, Computer Science Faculty Technische Universität Chemnitzn, 2006, https://nbn-resolving.org/urn:nbn:de:swb:ch1-200601972.

[67] M. Randrianarivony. On global continuity of Coons mappings in patching CAD surfaces. *Comput. Aided. Des.*, 41(11):782–791, 2009. https://doi.org/10.1016/j.cad.2009.04.012.

[68] E. Rank, M. Ruess, S. Kollmannsberger, D. Schillinger, and A. Düster. Geometric modeling, isogeometric analysis and the finite cell method. *Comput. Methods Appl. Mech. Engrg.*, 249–252:104–115, 2012. https://doi.org/10.1016/j.cma.2012.05.022.

[69] N. Ray, B. Vallet, L. Alonso, and B. Levy. Geometry-aware direction field processing. *ACM Trans. Graph.*, 29(1):Article No. 1, 2009. https://doi.org/10.1145/1640443.1640444.

[70] N. Ray, B. Vallet, W. C. Li, and B. Lévy. N-symmetry direction field design. *ACM Trans. Graph*, Article No. 10, 2008. https://doi.org/10.1145/1356682.1356683.

[71] M. Ruess, D. Schillinger, Y. Bazilevs, V. Varduhn, and E. Rank. Weakly enforced essential boundary conditions for nurbs-embedded and trimmed nurbs geometries on the basis of the finite cell method. *Internat. J. Numer. Methods Engrg.*, 95(10):811–846, 2013. https://doi.org/10.1002/nme.4522.

[72] M. Ruess, D. Schillinger, A. I. Özcan, and E. Rank. Weak coupling for isogeometric analysis of non-matching and trimmed multi-patch geometries. *Comput. Methods Appl. Mech. Engrg.*, 269:46–71, 2014. https://doi.org/10.1016/j.cma.2013.10.009.

[73] E. Sande, C. Manni, and H. Speleers. Sharp error estimates for spline approximation: Explicit constants, n-widths, and eigenfunction convergence. *Math. Models. Methods. Appl. Sci.*, 29(6):1175–1205, 2019. https://doi.org/10.1142/S0218202519500192.

[74] E. Sande, C. Manni, and H. Speleers. Explicit error estimates for spline approximation of arbitrary smoothness in isogeometric analysis. *Numer. Math.*, 144:889–929, 2020. https://doi.org/10.1007/s00211-019-01097-9.

[75] R. Schmidt, R. Wüchner, and K.-U. Bletzinger. Isogeometric analysis of trimmed NURBS geometries. *Comput. Methods Appl. Mech. Engrg.*, 241–244:93–111, 2012. https://doi.org/10.1016/j.cma.2012.05.021.

[76] T. W. Sederberg, D. C. Anderson, and R. N. Goldman. Implicit representation of parametric curves and surfaces. *Computer Vision, Graphics, and Image Processing*, 28(1):72–84, 1984. https://doi.org/10.1016/0734-189X(84)90140-3.

[77] T. W. Sederberg, G. T. Finnigan, X. Li, H. Lin, and H. Ipson. Watertight trimmed NURBS. In *ACM SIGGRAPH 2008 Papers*, SIGGRAPH '08, Article No. 79. ACM, 2008, https://doi.org/10.1145/1399504.1360678.

[78] T. W. Sederberg, J. Zheng, A. Bakenov, and A. Nasri. T-splines and T-NURCCSs. *ACM Trans. Graph.*, 22(3):477–484, 2003. https://doi.org/10.1145/882262.882295.

[79] J. Shen, J. Kosinka, M. Sabin, and N. A. Dodgson. Converting a CAD model into a non-uniform subdivision surface. *Comput. Aided Geom. Des.*, 48:17–35, November 2016. https://doi.org/10.1016/j.cagd.2016.07.003.

[80] K. M. Shepherd, R. R. Hiemstra, and T. J. R. Hughes. The quad layout immersion: A mathematically equivalent representation of a surface quadrilateral layout. *arXiv preprint arXiv:2012.09368*, 2020. https://arxiv.org/abs/2012.09368.

[81] J. R. Shewchuck. Triangle: Engineering a 2D mesh generator and Delaunay triangulator. In M. C. Lin and D. Manocha, editors, *Applied Computational Geometry Towards Geometric Engineering. WACG 1996. Lecture Notes in Computer Science*, volume 1148, pages 203–222. Springer, Berlin, Heidelberg, 1996, https://doi.org/10.1007/BFb0014497.

[82] J. R. Shewchuk. *Delaunay Refinement Mesh Generation*. PhD thesis, Carnegie Mellon University, 1997.

[83] J. R. Shewchuk. General-dimensional constrained delaunay and constrained regular triangulations, I: Combinatorial properties. *Discrete Comput. Geom.*, 39:580–637, March 2008. https://doi.org/10.1007/s00454-008-9060-3.

[84] A. Shtengel, R. Poranne, O. Sorkine-Hornung, S. Z. Kovalsky, and Y. Lipman. Geometric optimization via composite majorization. *ACM Trans. Graph.*, 36(4):Article No. 38, July 2017. https://doi.org/10.1145/3072959.3073618.

[85] J. Smith and S. Schaefer. Bijective parameterization with free boundaries. *ACM Trans. Graph.*, 34(4):Article No. 70, July 2015. https://doi.org/10.1145/2766947.

[86] D. C. Thomas, L. Engvall, S. Schmidt, K. Tew, and M. Scott. U-splines: splines over unstructured meshes. Technical report, Coreform, LLC, 2018, https://coreform.com/usplines.

[87] Y. Tong, P. Alliez, D. Cohen-Steiner, and M. Desbrun. Designing quadrangulations with discrete harmonic forms. In *Proceedings of the Fourth Eurographics Symposium on Geometry Processing*, SGP '06, pages 201–210. Eurographics Association, 2006, https://doi.org/10.2312/SGP/SGP06/201-210.

[88] B. Urick, B. Marussig, E. Cohen, R. H. Crawford, T. J. R. Hughes, and R. F. Riesenfeld. Watertight Boolean operations: A framework for creating CAD-compatible gap-free solid models. *Comput. Aided Design.*, 115:147–160, 2019. https://doi.org/10.1016/j.cad.2019.05.034.

[89] X. Wei, X. Li, K. Qian, T. J. R. Hughes, Y. J. Zhang, and H. Casquero. Analysis-suitable unstructured T-splines: Multiple extraordinary points per face. *arXiv preprint arXiv:2103.05726*, 2021. https://arxiv.org/abs/2103.05726.

[90] Y.-L. Yang, R. Guo, F. Luo, S.-M. Hu, and X. Gu. Generalized discrete Ricci flow. *Comput. Graph. Forum*, 28(7):2005–2014, 2009. https://doi.org/10.1111/j.1467-8659.2009.01579.x.

[91] X. Zheng, Y. Zhu, N. Lei, Z. Luo, and X. Gu. Quadrilateral mesh generation III: Optimizing singularity configuration based on Abel-Jacobi theory. *arXiv preprint arXiv:2007.07334*, 2020. https://arxiv.org/abs/2007.07334.

[92] Z. Zou, T. J. R. Hughes, M. A. Scott, R. J. Sauer, and E. J. Savithac. Galerkin formulations of isogeometric shell analysis: Alleviating locking with greville quadratures and higher-order elements. *Comput. Methods Appl. Mech. Engrg.*, 380:Article No. 113757, 2021. https://doi.org/10.1016/j.cma.2021.113757.

[93] Z. Zou, M. A. Scott, D. Miao, M. Bischoff, B. Oesterle, and W. Dornisch. An isogeometric Reissner–Mindlin shell element based on Bézier dual basis functions: Overcoming locking and improved coarse mesh accuracy. *Comput. Methods Appl. Mech. Engrg.*, 370:Article No. 113283, 2020. https://doi.org/10.1016/j.cma.2020.113283.